atmosphere

Article

Spatiotemporal Distribution Characteristics and Multi-Factor Analysis of Near-Surface $PM_{2.5}$ Concentration in Local-Scale Urban Areas

Lin Liu [1], Huiyu He [2], Yushuang Zhu [1,*], Jing Liu [3,*], Jiani Wu [1], Zhuang Tan [2] and Hui Xie [2]

[1] School of Civil and Transportation Engineering, Guangdong University of Technology, Guangzhou 510006, China; liulin@gdut.edu.cn (L.L.); 2112209041@mail2.gdut.edu.cn (J.W.)
[2] Shenzhen General Integrated Transportation and Municipal Engineering Design & Research Institute Co., Ltd., Shenzhen 518003, China; huiyu_he@163.com (H.H.); tz-207@163.com (Z.T.); xiehui7269@163.com (H.X.)
[3] School of Architecture, Harbin Institute of Technology, Harbin 150001, China
* Correspondence: 2112109125@mail2.gdut.edu.cn (Y.Z.); liujinghit@hit.edu.cn (J.L.)

Abstract: Near-surface $PM_{2.5}$ concentrations have been greatly exacerbated by urban land expansion and dense urban traffic. This study aims to clarify the effects of multiple factors on near-surface $PM_{2.5}$ concentrations from three perspectives of background climatic variables, urban morphology variables, and traffic-related emission intensity. First, two case areas covering multiple local blocks were selected to conduct mobile measurements under different climatic conditions. The observed meteorological parameters and $PM_{2.5}$ concentration were obtained through GIS-based imaging. These interpolation results of air temperature and relative humidity reveal highly spatiotemporal diversity, which is greatly influenced by artificial heat emissions and spatial morphology characteristics in local areas. The $PM_{2.5}$ concentration on measurement days also varies considerably from the lowest value of 44~56 μg/m^3 in October to about 500 μg/m^3 in December in Harbin winter and ranges between about 5 μg/m^3 and 50 μg/m^3 in Guangzhou summer. The correlation analysis reveals that both the climatic conditions and urban morphology characteristics are significantly correlated with local $PM_{2.5}$ concentration. Especially for Guangzhou summer, the $PM_{2.5}$ concentration was positively correlated with the street traffic emission source intensity with correlation coefficient reaching about 0.79. Multivariate nonlinear formulas were applied to fit the association between these factors and $PM_{2.5}$ concentration with higher determined coefficients. And optimization strategies are thus suggested to improve the urban air quality in local-scale areas. This attribution analysis contributes to environmentally friendly urban construction.

Keywords: $PM_{2.5}$ concentration; multi-factor; correlation analysis; local scale; climate regions

check for updates

Citation: Liu, L.; He, H.; Zhu, Y.; Liu, J.; Wu, J.; Tan, Z.; Xie, H. Spatiotemporal Distribution Characteristics and Multi-Factor Analysis of Near-Surface $PM_{2.5}$ Concentration in Local-Scale Urban Areas. *Atmosphere* **2023**, *14*, 1583. https://doi.org/10.3390/atmos14101583

Academic Editor: Miroslaw Zimnoch

Received: 18 September 2023
Revised: 12 October 2023
Accepted: 15 October 2023
Published: 19 October 2023

1. Introduction

$PM_{2.5}$ is a typical pollutant that contributes significantly to worldwide regional air pollution [1]. $PM_{2.5}$ pollution has become one of the most serious environmental pollution problems in built-up cities [2]. Near-surface $PM_{2.5}$ concentration has been proven to reduce sky visibility [3,4], deteriorate indoor and outdoor air quality, and cause a series of diseases [5,6]. Longtime exposure to $PM_{2.5}$, which can be inhaled directly into the alveoli of the lungs, is a major health hazard, resulting in increased cancer incidence and mortality [7]. Zhu et al. [8] discovered that the possibility of risk occurrence went up by 31.1–40.1% with every unit increase in $PM_{2.5}$ concentration. Liu et al. [9] found that long-term exposure to $PM_{2.5}$ leads to an increased incidence of asthma in adults. In addition, Zahed et al. [10], through real-time monitoring of old houses in Tehran, confirmed that the conditions of building windows and building leakage cause outdoor pollutants to worsen indoor air quality. Chen et al. [11] illustrated that indoor $PM_{2.5}$ emissions from outdoor sources caused 63.1% of all such deaths after multiple-path particle simulation.

In recent years, with the continuous expansion of urban land [12,13] and rapid increase in the number of vehicles [14], $PM_{2.5}$ pollution has worsened considerably [15] and the near-surface $PM_{2.5}$ concentration still far exceeds the WHO standard in many highly developed urban areas [16]. Therefore, the distribution characteristics and driving factors of near-surface $PM_{2.5}$ concentration deserve a detailed inspection to develop a control strategy for reducing $PM_{2.5}$ concentration and alleviating urban air pollution. Currently, there are sufficient studies illustrating the source and distribution of $PM_{2.5}$ in urban areas. Complex sources, including industrial sources [17], biomass burning [18], and traffic emissions [19,20], all contribute considerably. In addition, multiple factors are attributed to varying degrees of importance in influencing the dispersal and transmission of the near-surface $PM_{2.5}$ concentration, including meteorological factors [21,22] and urban spatial characteristics [23,24]. Table 1 presents a series of factors affecting the spatiotemporal distributions of urban $PM_{2.5}$ concentration in the existing articles. These factors are mainly divided into three aspects. The first is the emission sources of $PM_{2.5}$ concentration, mainly reflected by traffic-related emission sources and heating-related burning processes. The second is the climatic region diversity, which directly leads to the different meteorological parameters and results in different levels of condensation and transport of fine particulate matter. The third is the urban morphology heterogeneity, which is usually expressed by different building densities, building plot ratios, tree planting, etc.

Interestingly, although a few studies discussed the distribution characteristics and factors of urban $PM_{2.5}$ pollution, these studies usually focus on one single aspect. The factors of the three aspects generally have a combined effect on the near-surface $PM_{2.5}$ concentration. As shown in Figure 1, a large amount of particulate matter was produced by emission sources like traffic gas then dynamically transmitted to built-up urban blocks driven by background wind and then aggregated with different concentrations in different places associated with various urban spatial morphology. During the whole process, the different climatic regions usually have different underlying surface forms. In hot and humid climatic regions, the urban areas are covered with dense and tall trees and large ranges of green space under the high temperature and high humidity meteorological conditions. These typical underlying surface characteristics and hot–humid climatic conditions greatly influence the adsorption and sedimentation of the particulate matter. On the other hand, in the severe cold climatic region, the urban space is usually covered with thick layers of snow during long-term wintertime, and large amounts of industrial waste gas and straw burning and fuel usage from heavy-duty vehicles are prominent during the heating season. These specific life and production features also intensify the particulate matter emission. In addition, the urban construction intensity and development speed also varied considerably due to the different economic opportunities and population sizes in different cities.

Therefore, a common consensus has been reached that different climatic conditions and the associated urban morphology and emission intensity certainly affect the whole process of $PM_{2.5}$ production, transmission, and aggregation. This complicated process results in significant $PM_{2.5}$ distribution differences that vary with time and space.

The spatial difference of near-surface $PM_{2.5}$ concentration is related to the urban local-scale morphology features. A city block, usually seen as a basic urban construction unit, is marked by a certain degree of underlying surface homogeneity bound by streets. In this way, the city blocks ranging within a limited local area have significant urban spatial morphology features.Therefore, local-scale urban space variables play an important role in local climate formation, which then directly influences the transport and sedimentation of particulate matter. However, current research usually concentrates on one or two certain urban spatial parameters from the perspective of building cluster form or vegetation coverage. Comprehensive land cover variables have not been fully taken into consideration.

Table 1. A series of factors affecting the spatiotemporal distributions of urban $PM_{2.5}$ concentration.

Direction	Authors (Years)	Key Observations and Techniques	Factors
	Shith et al. (2019) [17]	Measurements of concentrations of $PM_{2.5}$ and its constituents vary from place to place, depending on the source identification of $PM_{2.5}$ by the hysplit model.	Industrial activities
	Weaver et al. (2019) [18]	Burning biomass in a house affected the air quality of the surrounding houses through home observations.	Biomass combustion
Sources of background $PM_{2.5}$ concentration	Jeong et al. (2019) [19]	The contribution of traffic-generated $PM_{2.5}$ sources may vary across location and time according to a comparison of source contributions between two near-road sites.	Exhaust emissions, brake wear, resuspension of road dust
	Askariyeh et al. (2020) [20]	The environmental impacts of $PM_{2.5}$ concentrations associated with traffic near roads were modeled by using regulatory guidelines.	Combustion, brake wear, tire wear, and resuspended dust
Climatic region diversity	Li et al. (2017) [21]	Meteorological factors influencing $PM_{2.5}$ accumulation, dispersion, and transport were identified with correlation analysis.	Air temperature, pressure, rainfall, relative humidity, wind speed, and wind direction
	Zhou et al. (2020) [22]	Seasonal differences of meteorological elements on $PM_{2.5}$ were identified with correlation analysis.	Relative humidity, air temperature, wind and boundary layer height
Urban morphology heterogeneity	Danek et al. (2022) [23]	The sources of air pollution in cities were analyzed through a complex geostatistical approach for spatiotemporal analysis of particulate matter (PM) concentrations.	Topography, meteorological variables,
	Zareba et al. (2023) [24]	Spatiotemporal patterns of air pollution were analyzed through unsupervised machine learning algorithms.	Weather conditions, traffic patterns, and industrial activity
	Tan et al. (2023) [25]	Correlation relationships between $PM_{2.5}$ concentration and urban compactness were found through the density concentration function (DCF) model.	Urban compactness
	Zhang et al. (2022) [26]	The three-dimensional spatial index and multiple linear regression were used to analyze the relationship between three-dimensional urban form and $PM_{2.5}$ concentration at street level using a satellite-derived surface dataset.	Street accessibility, road length, terrain, urban vegetation, surrounding open green space, and transportation facilities

Based on the above issues, a clear understanding of spatiotemporal distribution characteristics of near-surface $PM_{2.5}$ concentration in local-scale urban areas needs better integration of multi-factor analysis. This study aims at the comprehensive influential factors, selecting two typical cities with totally different climatic conditions and locally representative built-up urban morphology features as comparative research objects. Mobile measurements for near-surface $PM_{2.5}$ concentration along designed routes covering typical built-up blocks were conducted during typical climatic conditions. The spatiotemporal patterns of near-surface $PM_{2.5}$ concentration were displayed by GIS-based imaging. Then, multiple factors were focused on, and their different impacts on $PM_{2.5}$ concentration distribution were determined through correlation analysis. This study contributes to clarifying the integration effects of multiple factors on $PM_{2.5}$ concentration and providing a theoretical basis for city air quality optimization.

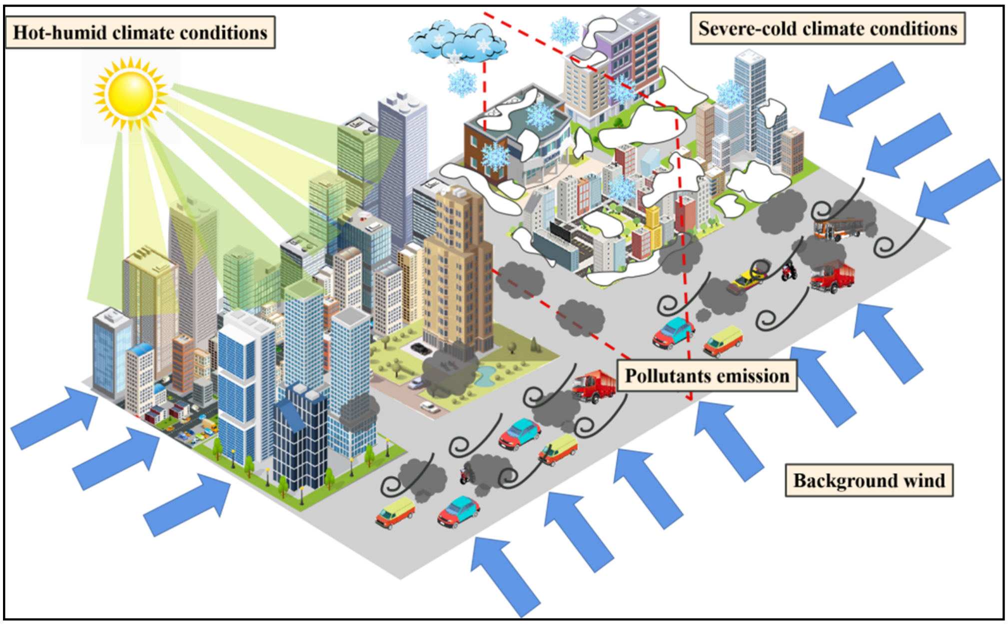

Figure 1. Complex combined effects of multiple factors affecting urban $PM_{2.5}$ distribution.

2. Methodology

2.1. Study Area

Considering the comprehensive factors from multiple perspectives, two typical cities from different climatic regions were selected, namely Harbin and Guangzhou. The two cities are in the severe-cold climate region and hot–humid climate region, respectively. This indicates that they have different built-up urban morphology and different emission sources.

Harbin is in Heilongjiang Province, Northeast China, between 125°42′~130°10′ east longitude and 44°04′~46°40′ north latitude near the Arctic Circle (see Figure 2). The air temperature in Harbin varies considerably throughout the year. During winter, the lowest temperature can drop to −38.1 °C, while the maximum air temperature can reach 36 °C during summer. Additionally, more than half of the year, air temperature is lower than 0 °C (Figure 3).

Guangzhou is in Guangdong Province in the southern coastal region of China, between 112°57′~114°03′ east longitude and 22°26′~23°56′ north longitude (see Figure 2). Guangzhou is also located in a typical subtropical climate, with an average annual air temperature of 20–22 °C and minor fluctuations in air temperature all over the year. The winter low temperature ranges from 4 °C to 6 °C, while the summer high temperature can reach up to 38 °C. About two-thirds of the year's months experience air temperatures above 30 °C (Figure 3). Therefore, the two cities have significant geographical and climatic differences. This suggests they could provide typical climatic variables.

Subsequently, to explore the impacts of local-scale urban morphology on the near-surface $PM_{2.5}$ concentration, typical built-up urban areas in Qiu Lin (QL) of Harbin and Pearl River New Town (PRNT) of Guangzhou (Figure 2) were selected in this study. The QL areas are mainly covered with middle-rise buildings with different spatial forms. PRNT is a typical central business district (CBD) with densely built high-rise official buildings and residential buildings. Then, QL and PRNT were divided into 11 and 8 blocks according to the underlying surface homogeneity characteristics and time-varying traffic flow patterns (see Figure 2).

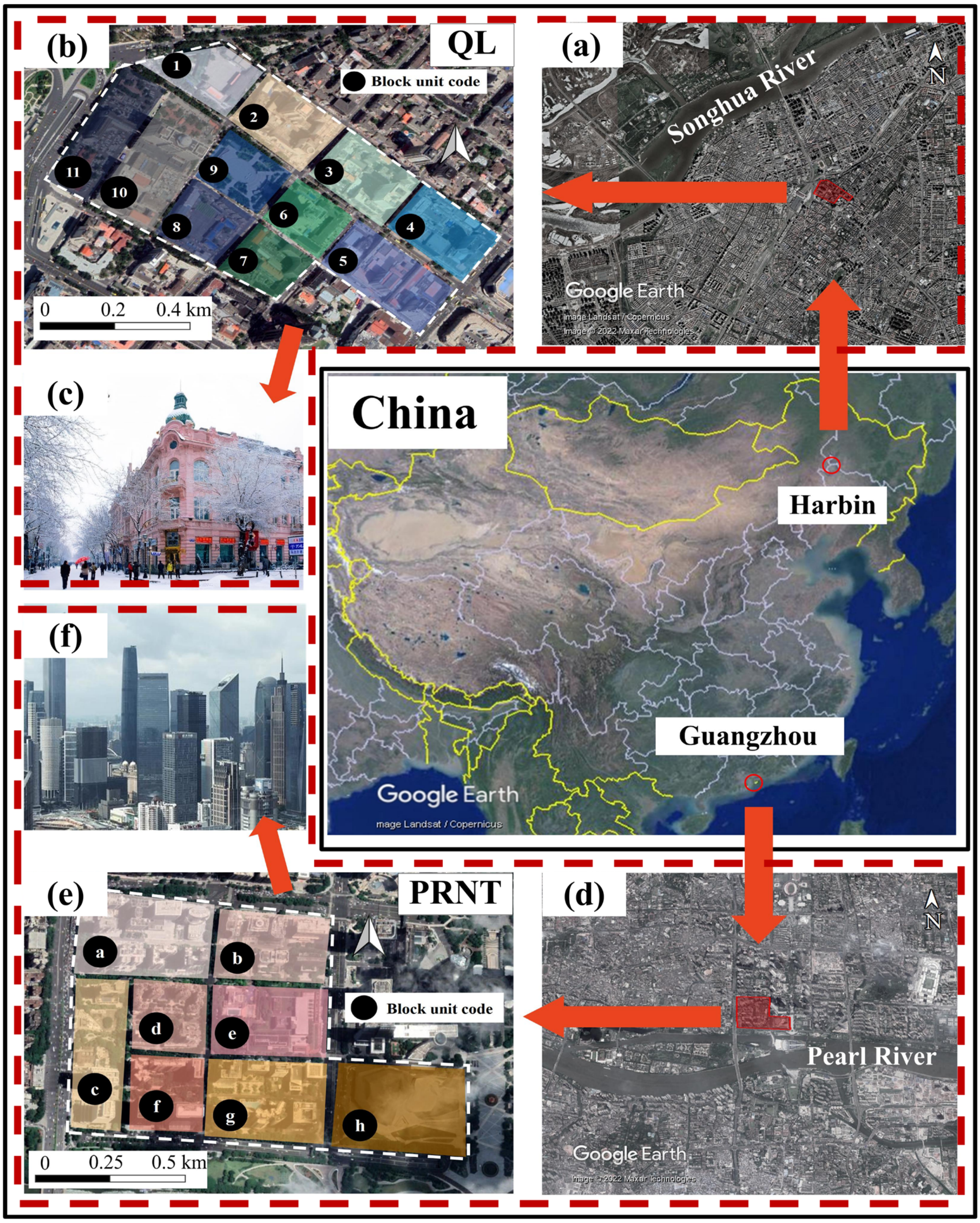

Figure 2. (**a**) The locations of regions in Harbin; (**b**) divided urban blocks in Harbin; (**c**) morphology scenes of the research areas in Harbin; (**d**) the locations of regions in Guangzhou; (**e**) divided urban blocks in Guangzhou; (**f**) morphology scenes of the research areas in Guangzhou.

To quantify the urban spatial morphology characteristics, several urban surface characteristic parameters of the urban block should be determined as influential urban morphology factors. Referring to the existing studies on the local climate zone (LCZ) scheme [27,28], the involved parameters include the sky view factor (*SVF*), aspect ratio of street canyon (*AR*), height of roughness elements (*HRE*), building surface fraction (*BSF*) and normalized difference vegetation index (*NDVI*). The calculation methods are shown in Table 2 (the detailed information was shown in reference [29]).

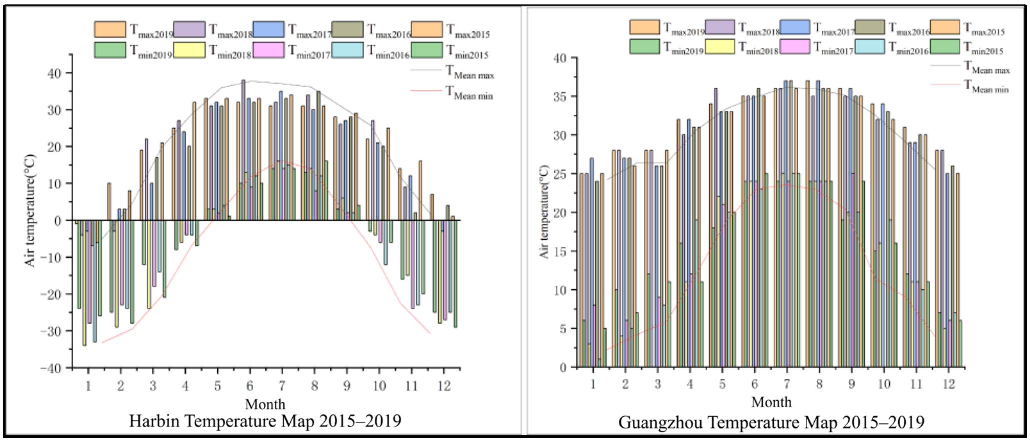

Figure 3. Annual air temperature variations of Harbin and Guangzhou.

As shown in Table 2, *SVF* [30] is the dimensionless value that is used to describe the proportion of the sky or open canyon space of the urban street valley course. The *SVF* value ranges from 0 to 1. The larger the *SVF* value, the higher the visibility of the sky. *AR* [31] and *HRE* [32] are the important elements to determine the spatial scale of the street. *BSF* [33] is the ratio of the total area of each building and structure in the region to the total area of the region. *BSF* can be calculated by processing satellite image data; the higher its value, the higher the building density in the region. *NDVI* [34] is related to vegetation cover m, which can reflect the influences of plant canopy. The values of *NDVI* were obtained from satellite imagery data.

Table 2. Calculation method of surface morphology characteristic parameters.

Surface Factor	Methods Adopted	Calculation Method	Explanation
Sky view factor (*SVF*)	Photographs filmed by fish-eye camera	$SVF = \frac{S_{sky}}{S_{total}}$	S_{sky} is the visible sky area in a fish-eye photograph, m^2. S_{total} is the total circular area of a fish-eye photograph, m^2.
Aspect ratio of street canyon (*AR*)	Data recording from field surveys	$AR = \frac{H}{W}$	H is the height of the street canyon in the block, m. W is the width of the street canyon in the block, m.
Height of roughness elements (*HRE*)		$HRE = \frac{\sum_{i=1}^{n} h_i}{n}$	h_i is the height of the building in the block, m. n is the number of buildings in the block.
Building surface fraction (*BSF*)	Satellite imagery data from Google Earth	$BSF = \frac{S_b}{S_{total}}$	S_b represents the outline area of the building base in the block, m. S_{total} is expressed as the total area of the block.
Normalized difference vegetation index (*NDVI*)		$NDVI = ((IR - R)/(IR + R))$	IR is the pixel value of the infrared band. R is the pixel value of red-light band.

2.2. Mobile Monitoring Routes and Instrument Settings

In this study, mobile surveys were conducted in Harbin during the winter periods (October, November, and December) in 2021 and in Guangzhou during the summer periods (May, June, and July) in 2022. Then, we obtained the multi-spatiotemporal $PM_{2.5}$ concentration data in different urban areas under typical meteorological conditions. As shown in Figure 4a, these areas have obvious differences in building layout and street specifications. Hence, the mobile routes are carefully designed to cover most research areas across QL and PRNT, as shown in Figure 4b. Two closed mobile routes, passing through the entire study area, are finally determined to ensure the accuracy of the simultaneous data correction. During the mobile survey, the fixed stations were set up to monitor the background climatic variations and background $PM_{2.5}$ concentration variations within the study areas, as shown in Figure 4b.

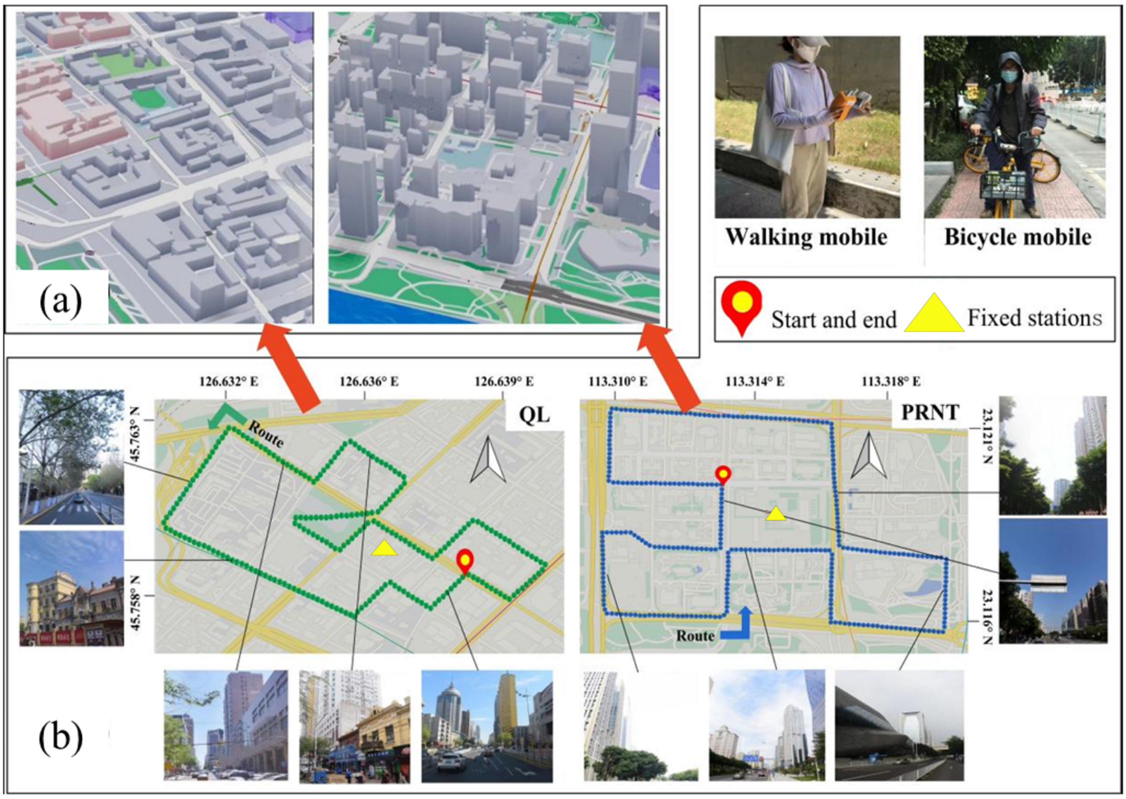

Figure 4. (**a**) Three-dimensional views of the two study areas in QL and PRNT; (**b**) monitoring routes and field scenes of the two study areas.

According to the pre-experiments, field data show that traffic flow has typicality and a certain density at four typical moments of the day (namely the 9:00, 11:00, 13:00, and 15:00). Taking the traffic-related $PM_{2.5}$ emission as the main influential emission source, four rounds of continuous mobile monitoring were conducted along the mobile routes with a starting time point at 9:00, 11:00, 13:00, and 15:00 on each measurement day. To avoid the interference of vehicle gas with test data, slow mobile monitoring modes like walking and bicycling were adopted at an even mobile speed. The whole mobile survey time was controlled within 40 min to avoid dramatic changes in background environment data. The selection of fixed stations should avoid direct sunlight and human disturbance.

The mobile survey equipment utilized was a hand-held particulate matter detector (GT-1000) and HOBO U23-002 portable temperature and humidity sensor as monitoring devices to record the near-surface $PM_{2.5}$ concentration variations and the corresponding simultaneous air temperature and humidity data along the mobile route. In addition, a handheld Beidou terminal was also equipped to record the latitude and longitude coordinates of the measuring points on the mobile route. The location data for each test point on the mobile route can correspond to the air temperature, relative humidity, and $PM_{2.5}$ concentration, which is convenient for the subsequent visual processing of these test data on the geographic information system (GIS) platform. Fixed stations including a GRIMM particulate matter detector and a fixed HOBO U23-002 were used for real-time monitoring of air temperature, humidity, and $PM_{2.5}$ concentration at the fixed sites. The specific parameters and settings of these instruments are shown in Table 3.

Table 3. Specific parameters and settings of instruments.

	Mobile Survey			**Fixed Observation Site**	
Instrument settings					
	GPS module (Intelligent Terminal A8)	Hand-held $PM_{2.5}$ detector (GT-1000-B3)	Temperature and humidity recorder (HOBO U23-002)	Fixed weather station (HOBO U23-002)	Particulate matter detector (GRIMM)
Monitoring data	Latitude and longitude	$PM_{2.5}$ concentration	Air temperature and relative humidity	Air temperature and relative humidity	$PM_{2.5}$ concentration
Test interval	1 s			1 min	
Accuracy	Single point (2–5 m)	±3%	±0.18 °C for air temperature; ±2.5% for relative humidity		Full scale ±5%

2.3. Climatic Conditions on Measurement Days and Data Processing

- *Background climatic conditions*

Fully considering the comprehensive meteorological conditions, six typical measurement days were selected, which included the heating days from October to December in Harbin and the cooling days from June to August in Guangzhou. In Figure 5, the background air temperature and relative humidity data at four moments during these measurement days are displayed with the fixed weather stations. These data distributions show that the air temperature greatly declined, varying from 2~8 °C in October to −16~−10 °C in December in Harbin with lower relative humidity data below 40%, which reveals a typical freezing cold winter condition. In Guangzhou, the air temperature mainly ranged from 29 °C to 38 °C with higher relative humidity data over 85%, which emphasized high temperature and high humidity weather conditions. Therefore, the selected measurement days meet the requirements of a wide range of meteorological differences and obvious climate zone differences, which could provide a better climatic comparison basis for further factor analysis.

- *Mobile data calibration*

Because the mobile data obtained by portable instruments have the problem of temporal non-simultaneity, the observed mobile data should be subjected to temporal simultaneity correction. Since the fixed stations are continuously monitored, the data from fixed stations can be used as basic benchmark data to conduct mobile data correction. A "Single" temporal correction method was carried out in this study on the observed mobile data [35,36]. As displayed in Figure 6, mobile data calibration for air temperature, relative humidity, and $PM_{2.5}$ concentration can be conducted.

The theoretical calibration was then carried out according to Equation (1).

$$A_{i\tau} = M_{i\tau} - (F_\tau - F_0) \quad (1)$$

where $A_{i\tau}$ is the calibrated mobile parameter of the mobile point i at time τ, $M_{i\tau}$ is the mobile parameter of the mobile point i at time τ, F_τ is the fixed parameter at the fixed station at time τ, and F_0 is the fixed parameter value at the fixed station at the initial time of one round of continuous mobile monitoring. In this way, the observed data could be modified and calibrated to a united time moment of 9:00, 11:00, 13:00, and 15:00 for spatial comparison.

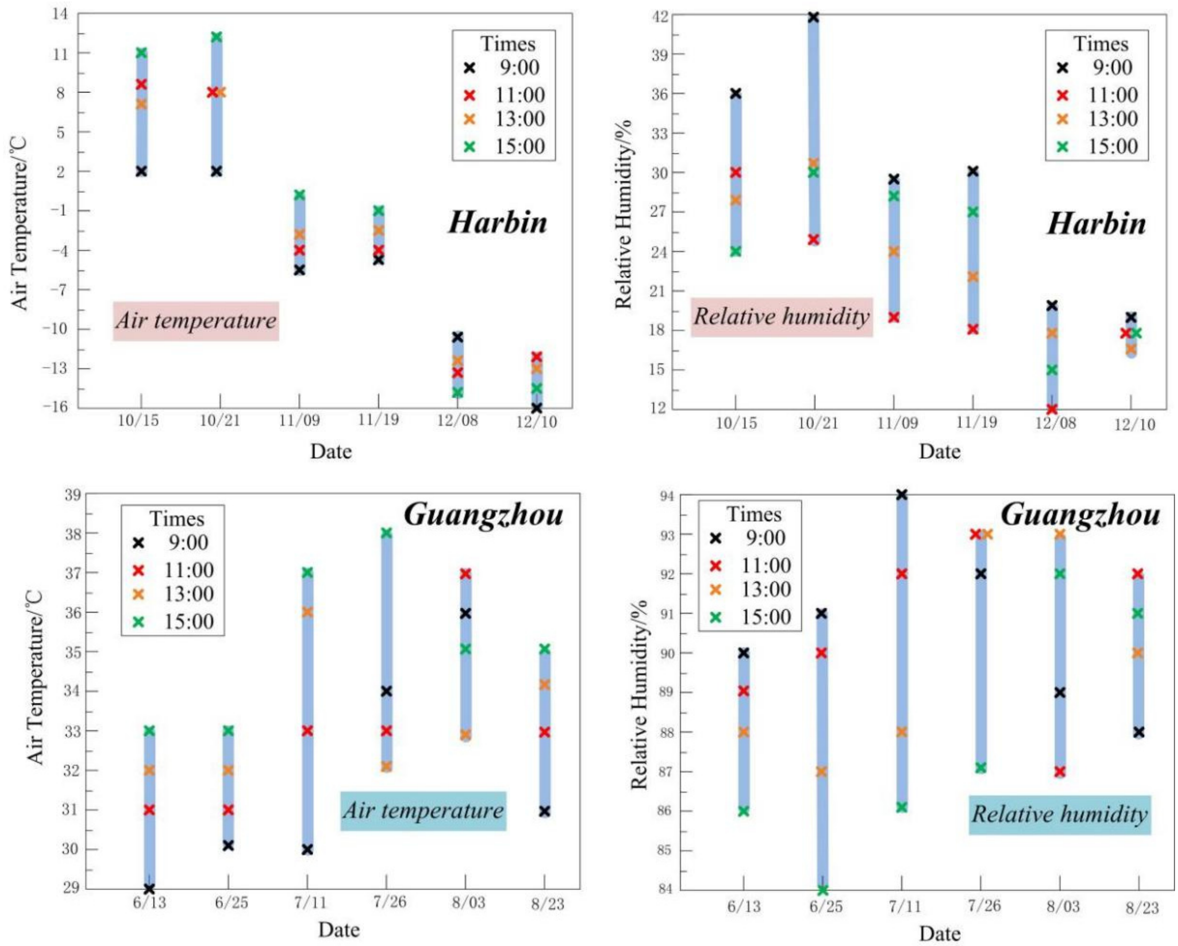

Figure 5. Background air temperature/relative humidity variations at four moments during the typical measurement days in Harbin and Guangzhou.

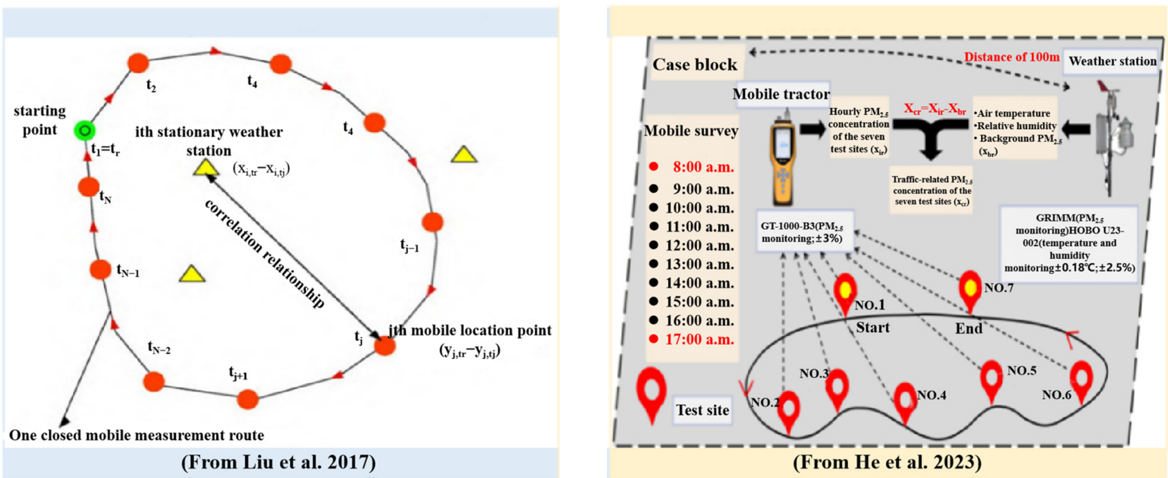

(**a**) (**b**)

Figure 6. (**a**) Temporal correction method description [35]; (**b**) data processing for the mobile $PM_{2.5}$ observation [36].

- *Factor collection*

As shown in Figure 1, this study considered three perspectives of factors as independent variables to analyze their impacts on near-surface $PM_{2.5}$ concentration. Based on the above field survey, these factors include climatic variables of background air temperature (AT) and relative humidity (RH); five urban morphology variables of sky view factor (SVF), aspect ratio of street canyon (AR), height of roughness elements (HRE), building surface fraction (BSF), and normalized difference vegetation index ($NDVI$); and the hourly background $PM_{2.5}$ concentration (BC) (mainly the traffic-related emission source).

Among these factor variables, the traffic emission at the pedestrian level was evaluated. First, the hourly traffic volume of each road around the study block units was monitored and counted, including the types of vehicles passing through a road section per hour and the corresponding number. The $PM_{2.5}$ emission source intensity (ESI) can be calculated as Equations (2)–(4). Equation (2) is the traffic-related emission from factor analysis, Equation (3) is the calculation of dust emission proposed by the EPA, and Equation (4) represents the combined emission covering Equations (1) and (2).

$$Q_V = E \cdot C \tag{2}$$

$$Q_Y = \left[k \left(\frac{sL}{2} \right)^{0.65} * \left(\frac{W}{3} \right)^{1.5} \right] C \tag{3}$$

$$ESI = Q_V + Q_Y \tag{4}$$

where Q_V is the emission intensity of the traffic line source, $\mu g/(m \cdot s)$. Q_Y is the emission intensity of the $PM_{2.5}$ dust source, $\mu g/(m \cdot s)$. ESI is the emissions that combine traffic and dust in $\mu g/(m \cdot s)$. E is the $PM_{2.5}$ emission factor, $mg/(veh \cdot km)$. C is the traffic volume per hour, veh/h. k is the dust emission coefficient and is set to 0.15 for $PM_{2.5}$ [37]. sL is the road dust load and is set to 0.3 for Guangzhou [38], g/m^2. W is the average vehicle weight of running vehicles; it is calculated by the vehicle weight and proportion of each vehicle type. In this way, these factors could be measured and collected.

- *Data processing*

Since the local-scale areas have homogeneous underlying surface characteristics, the spatiotemporal distributions of near-surface $PM_{2.5}$ concentration in these city blocks were mainly focused on. After importing the corresponding coordinates of AT, RH, and $PM_{2.5}$ concentration of the continuous points into the ArcGIS platform, the interpolation of them could be obtained through Geostatical Analyst. According to Liu et al. [39], three typical kinds of interpolation methods, namely kriging, inverse distance-weighted (IDW), and spline, were compared. Among them, the kriging interpolation method has been proved to be suitable for mobile $PM_{2.5}$ data processing. The overall interpolation accuracy can be evaluated according to root mean square and standard root mean square.

Based on the above interpolation results, the Spatial Analysis tool of the ArcGIS platform was used to obtain statistics on the average value according to the divided block units. Thus, the average values of near-surface $PM_{2.5}$ concentration and background AT/RH in each block unit at different time moments could be obtained. Since there are different dimensions between different variables, it is necessary to normalize the initial data. The z-score method, also known as the standard score method, is a process in which the difference between the score and the mean is divided by the standard deviation. The resulting z-value represents the distance between the original score and the maternal mean and is calculated in units of standard deviation, with z being negative when the original score is less than the mean and positive if the original score is greater than the mean. The variable values after processing are $z(PM_{2.5})$, $z(AT)$, $z(RH)$, $z(BC)$, $z(ESI)$, $z(SVF)$, $z(AR)$, $z(HRE)$, $z(BSF)$, and $z(NDVI)$. In this study, Spearman's correlation coefficient and p-value were used to determine the correlation relationships between $z(PM_{2.5})$ and each factor. Normalized $z(PM_{2.5})$ was taken as the dependent variable in this study, with $z(AT)$, $z(RH)$, $z(BC)$, $z(ESI)$, $z(SVF)$, $z(AR)$, $z(HRE)$, $z(BSF)$, and $z(NDVI)$ of each block unit as independent variables, and the nonlinear fitting equations were constructed. Finally, the optimal variables with the goodness of fit were used to construct the $PM_{2.5}$ multivariate nonlinear equations. The data processing and factor analysis are shown in Figure 7.

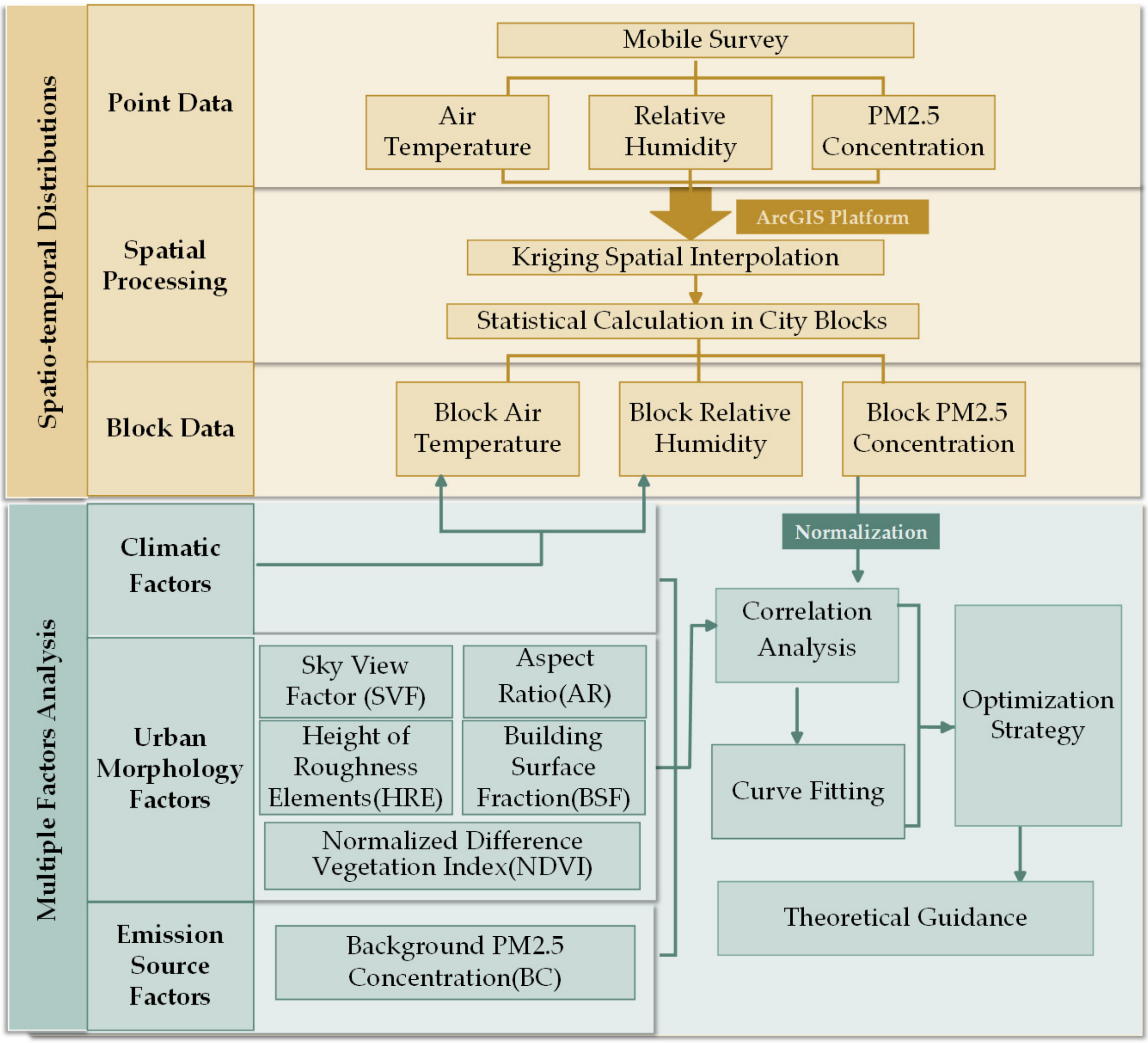

Figure 7. Flowchart of the data processing method for multi-factor analysis.

3. Results

3.1. Spatiotemporal Characteristic Distributions of Air Temperature

Figure 8 shows the spatial distribution of air temperature at four moments in the QL research area in Harbin during the wintertime. To highlight the spatial difference of parameters in city blocks, different series of color legends are applied to different months. The overall temperature varied from the higher air temperature level in October to the lower air temperature level in December. The air temperature of the two measured days in October was the lowest at 9 o'clock and reached the highest at 15 o'clock. The maximum temperature difference occurred at 15:00 on December 8th. The highest temperature in blocks was −9 °C, and the lowest temperature reached −16 °C. The overall spatial distribution was high in the east and low in the west, and the temperature in the northeast region was the highest. There was an obvious difference between the southeastern area and the surrounding area, which may be related to the existence of artificial heat emissions.

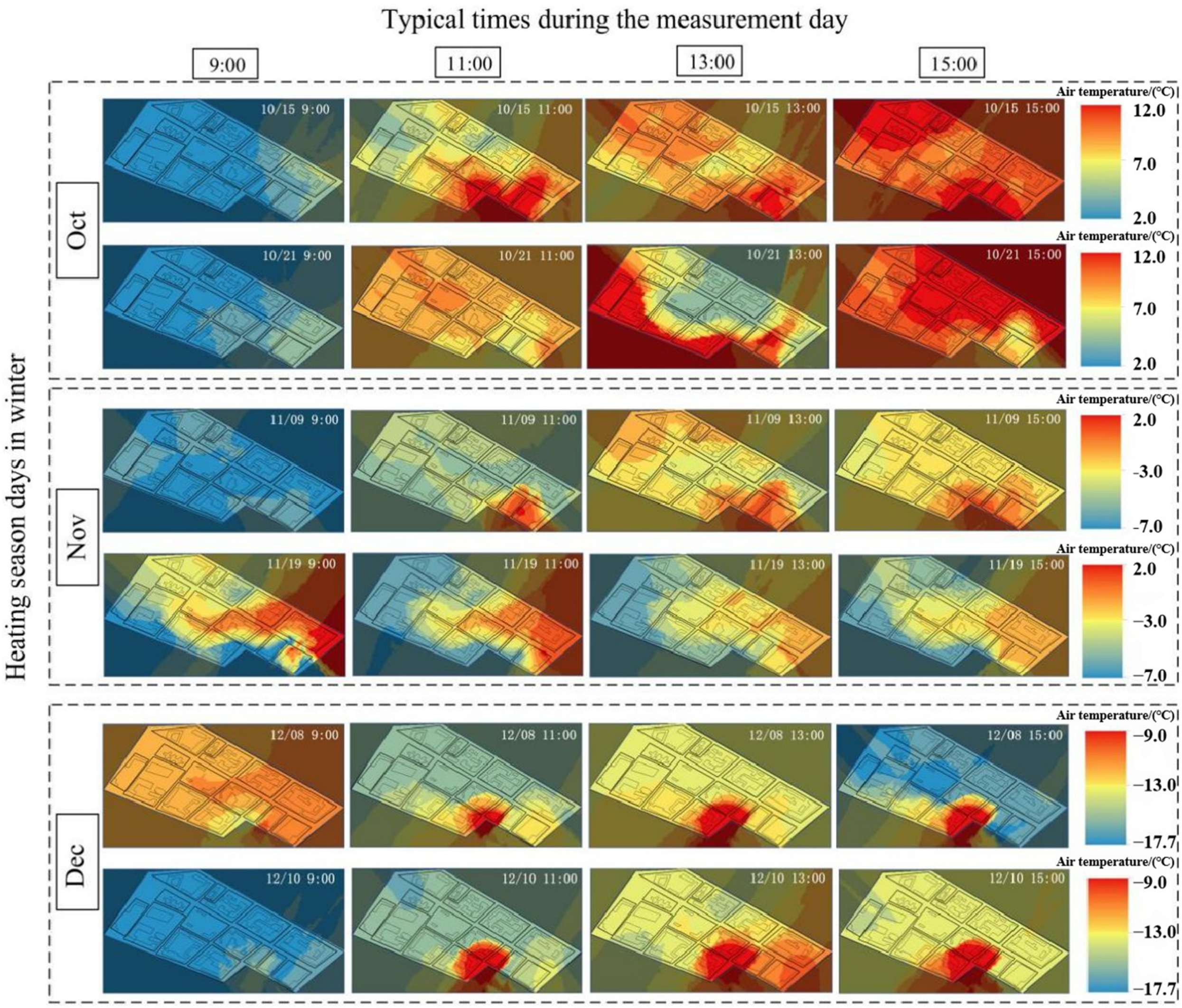

Figure 8. Spatiotemporal distributions of air temperature in QL study area in winter.

Figure 9 shows the spatial distribution of air temperature at four moments in the PRNT research area in Guangzhou during the summertime. The average air temperature in the study area was the maximum in August but the minimum in June. From a spatial perspective, as the background temperature increased, the air temperature in the east of the study area increased sharply, while the temperature increased relatively slowly in the interior of the study area, especially in the area with dense buildings, where the sunlight was difficult to direct directly due to the relatively large aspect ratio of the street.

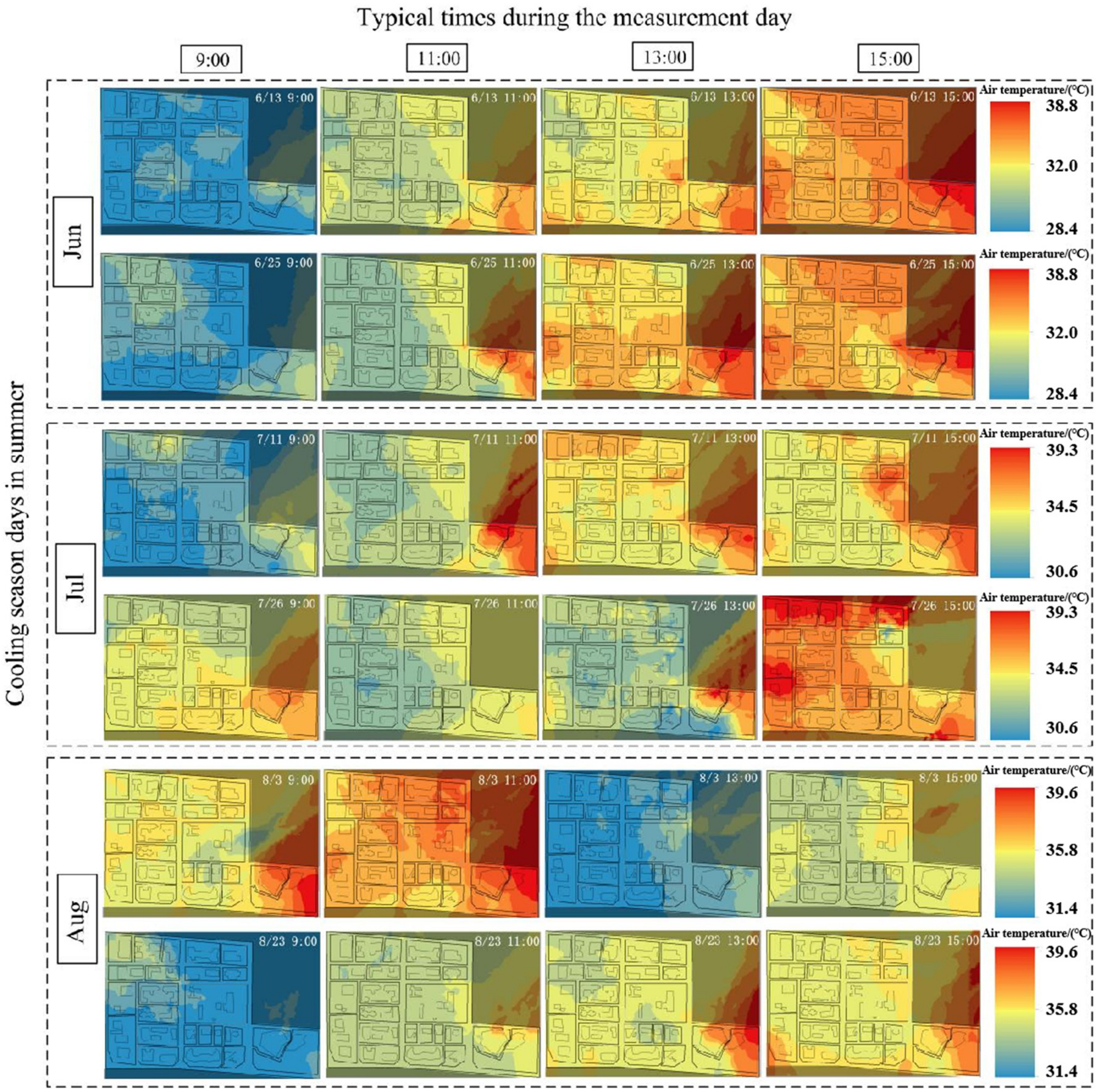

Figure 9. Spatiotemporal distributions of air temperature in PRNT study area in summer.

3.2. Spatiotemporal Characteristic Distributions of Relative Humidity

The spatial distribution of relative humidity in QL of Harbin is shown in Figure 10. The overall relative humidity in December was lower than that in October and November, and the lowest value of 8.7% occurred on 8 December. The spatial variation in humidity showed the objective law of high temperature and low humidity. The spatial distribution of humidity tends to be consistent with the increase in temperature. The phenomenon of high temperature and high humidity occurred on the north side of the blocks, which was characteristic of the lower *SVF* value and the higher *AR* value. So, the insufficient solar radiation led to the decrease in water evaporation in the air.

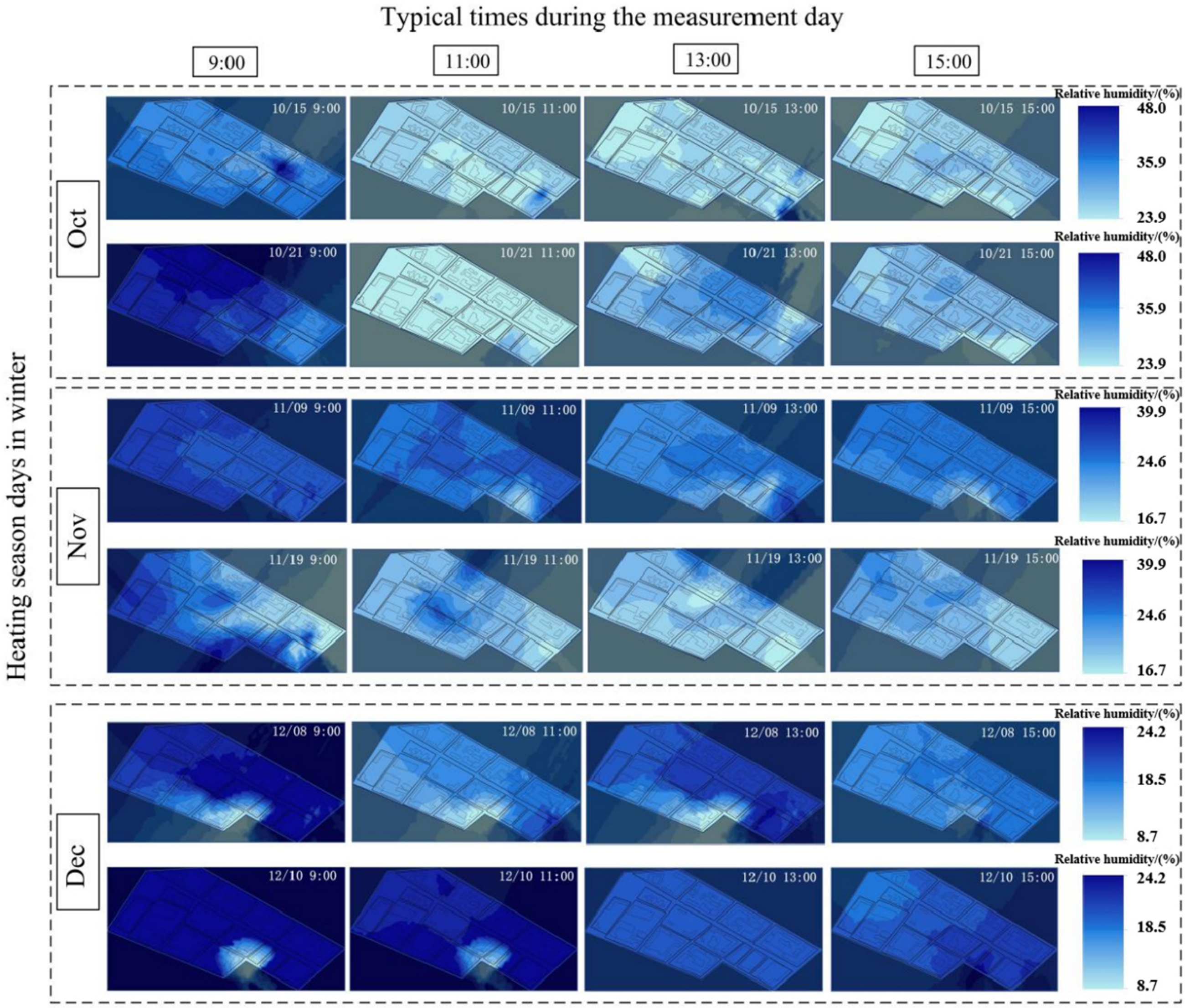

Figure 10. Spatiotemporal distributions of relative humidity in QL study area in winter.

Figure 11 shows the spatial distribution of relative humidity at four moments in the PRNT study area in Guangzhou during the summertime. Largely influenced by the background environment, the relative humidity in August was higher than that in June and July. And there was a minimum value of relative humidity ranging from 71% to 75% on 26 July, the lowest value of which occurred at 3 p.m. The overall distributions of relative humidity indicate higher values in the west and lower values in the east, and the areas with higher humidity were generally characterized by high building density and building height.

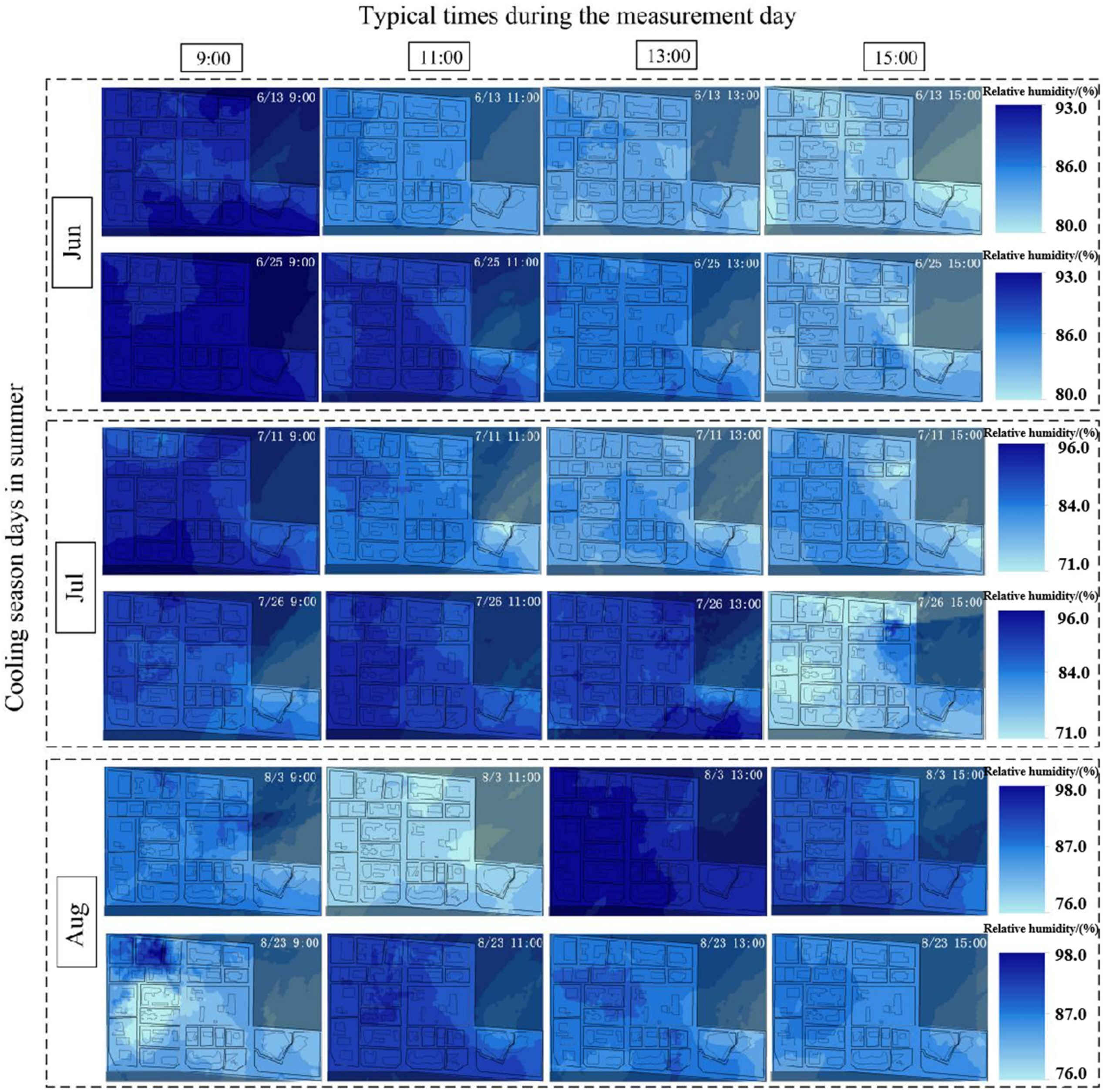

Figure 11. Spatiotemporal distributions of relative humidity in PRNT study area in summer.

3.3. Spatiotemporal Characteristic Distributions of $PM_{2.5}$ Concentration

The spatial distribution of near-surface $PM_{2.5}$ concentration at four moments in the QL research area in Harbin during the wintertime is shown in Figure 12. Due to the influence of the background concentration, the concentration range of the measurement days varies widely. The $PM_{2.5}$ concentration of 44~56 μg/m^3 was the lowest at 3 p.m. on October 15, while concentrations close to 300 μg/m^3 appeared in part of QL blocks on November 19th. From a spatial perspective, the $PM_{2.5}$ distribution was high in the west and low in the east, which was consistent with the direction of the background wind. According to the results on 8 and 10 December, the concentration of the eastern region deteriorated promptly, and traffic-related pollutants hardly diffused due to the high aspect ratio of buildings and their large proportion.

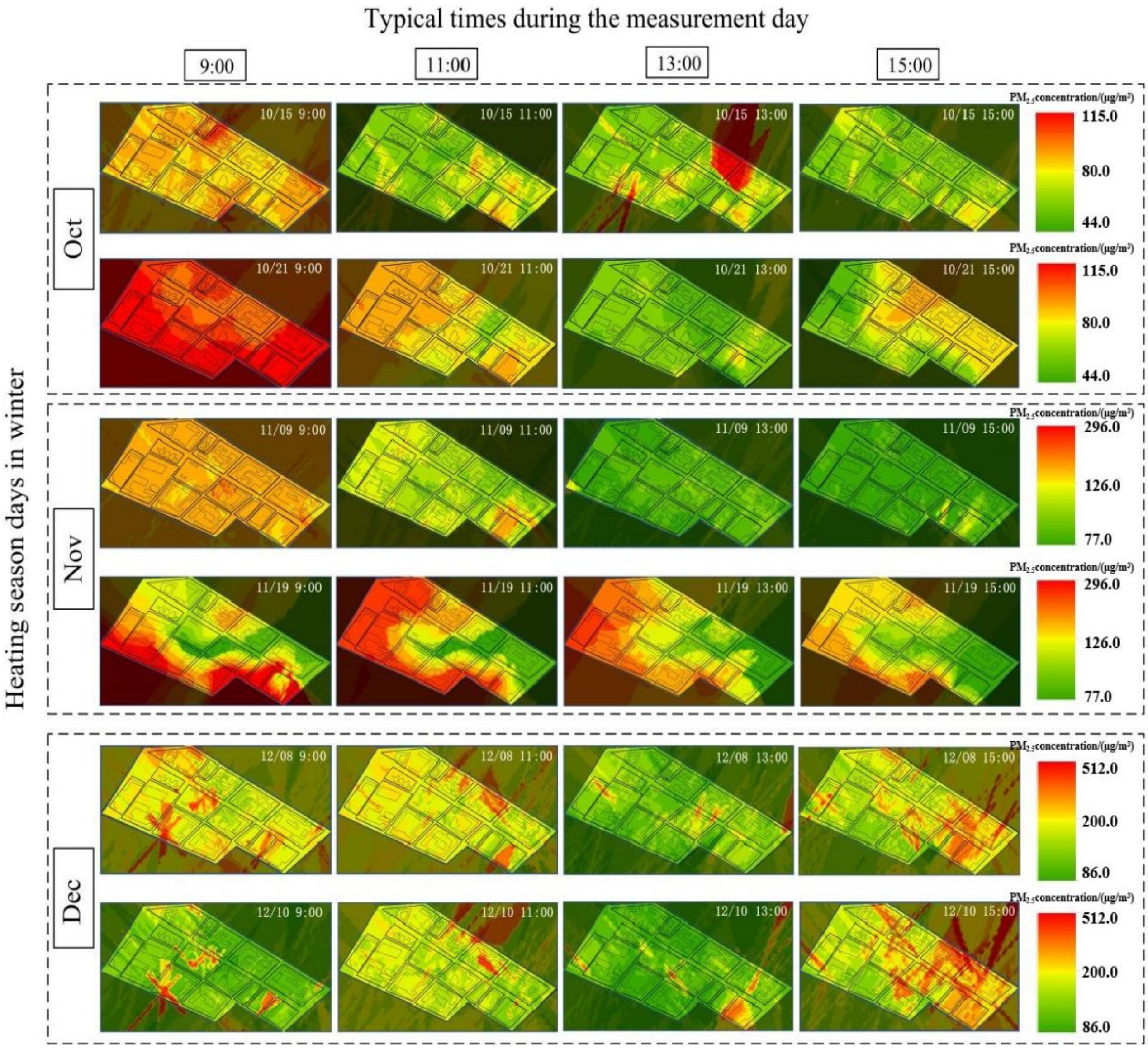

Figure 12. Spatiotemporal distributions of near-surface $PM_{2.5}$ concentration in QL study area in winter.

Figure 13 shows the spatial distribution of near-surface $PM_{2.5}$ concentration at four moments in PRNT of Guangzhou during the summertime. The overall concentration was far lower than that in Harbin. The time-varying characteristics of the concentration were consistent with the trend of the urban background concentration during the measurement days. The concentration of $PM_{2.5}$ was significantly different in spatial distribution. The lowest concentration of 3~12 $\mu g/m^3$ occurred in the areas with high plant coverage and high sky visibility factor. However, the distribution of $PM_{2.5}$ diffused radially in some areas, and the corresponding concentration reached 42~51 $\mu g/m^3$, which was related to the dense buildings and the continuous large amount of traffic emissions.

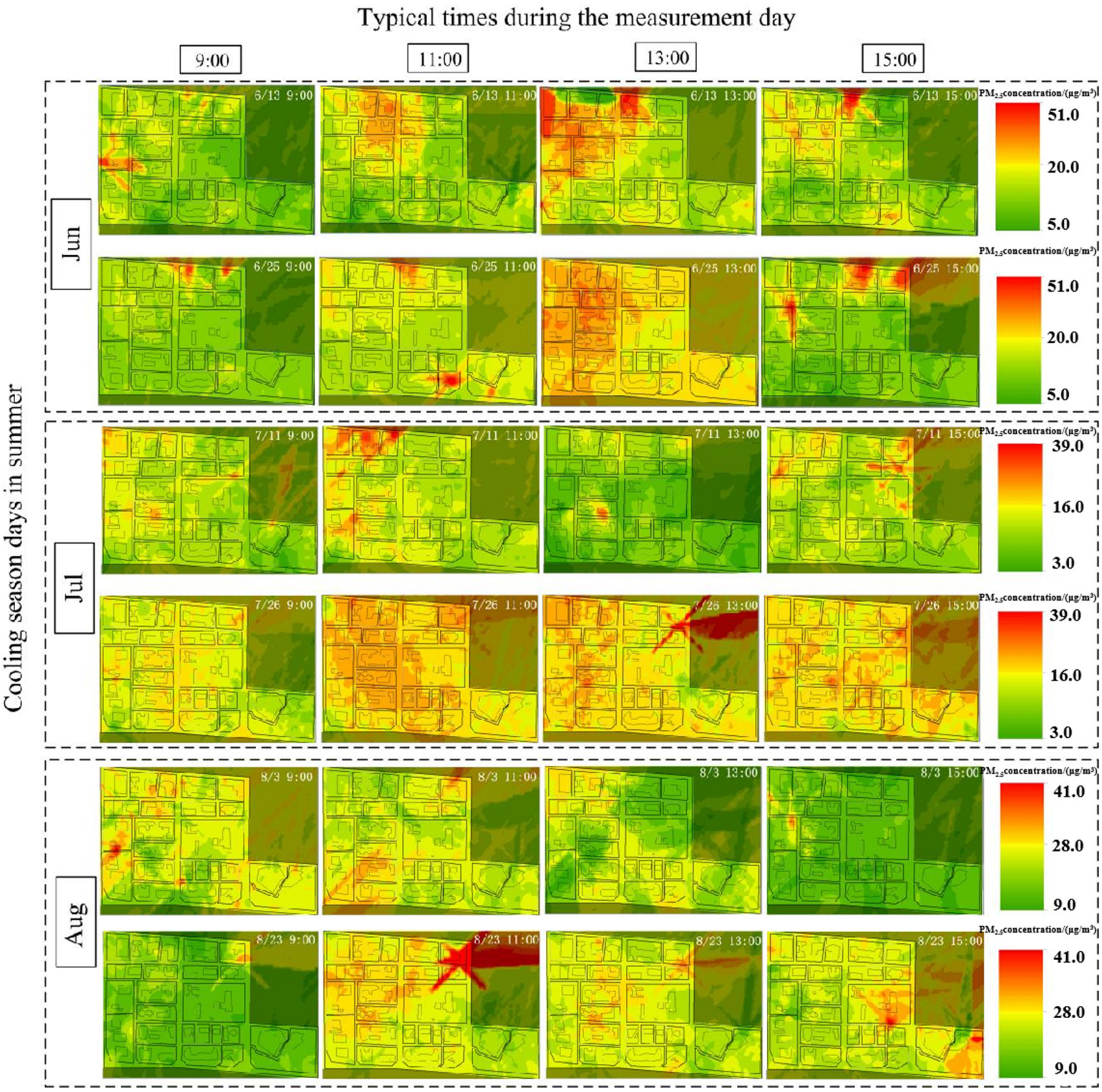

Figure 13. Spatiotemporal distributions of near-surface $PM_{2.5}$ concentration in PRNT study area in summer.

4. Discussion

4.1. Comparative Analysis of Multiple Factors Influencing Near-Surface $PM_{2.5}$ Concentration

Figure 14 reflects the correlation coefficients between $PM_{2.5}$ concentration and variables at different times during winter in Harbin and summer in Guangzhou. Overall, the $PM_{2.5}$ concentration in urban blocks of Harbin in winter is significantly correlated with *AT* and *RH* at the 0.01 significance level and significantly correlated with *SVF*, *HRE*, and *BSF* at the 0.05 significance level. The $PM_{2.5}$ concentration in Guangzhou summer was significantly correlated with air temperature and humidity at the 0.01 significance level and significantly correlated with *ESI*, *SVF*, *AR*, and *NDVI* at the significance level of 0.05.

As shown in Figure 14a, in Harbin winter, there was a high negative correlation between $PM_{2.5}$ concentration and *AT* most of the time. The value of the correlation coefficient was higher than 0.8 at certain moments (15:00 on 15 October, 9:00 and 15:00 on 21 October, 15:00 on 19 November, and 9:00 on 10 December). However, there was a strong negative correlation between $PM_{2.5}$ concentration and *RH* on 19 November. But at other times, the correlation between air humidity and $PM_{2.5}$ concentration was not so obvious.

Moreover, the $PM_{2.5}$ concentration was negatively correlated with *SVF*, and all were greater than 0.6 on 19 November. $PM_{2.5}$ concentration was then positively correlated with

HRE and *BSF*, with the maximum correlation coefficients of 0.69 and 0.6. In addition, there was no significant correlation between $PM_{2.5}$ concentration and *ESI*, *AR*, and *NDVI*. The $PM_{2.5}$ concentration in Harbin blocks in winter was less influenced by the traffic emissions and limited by the influence of street aspect ratio and plants.

As shown in Figure 14b, there was a high negative correlation between $PM_{2.5}$ concentration and air temperature at several moments in Guangzhou summer (13:00 and 15:00 on 13 June, 11:00 on 11 July, 9:00, 11:00, and 13:00 on 3 August). There was also a high positive correlation between $PM_{2.5}$ concentration and relative humidity at several moments, with the highest correlation coefficient being 0.91 on 13 June.

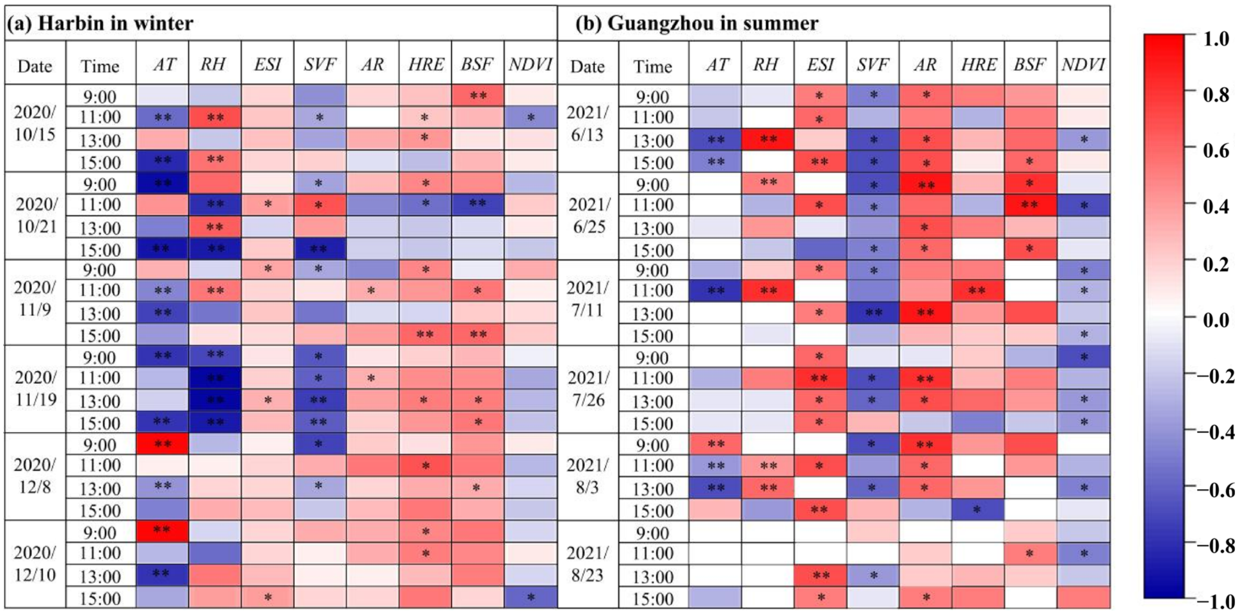

Figure 14. Correlation coefficients between $PM_{2.5}$ concentration and variables at different times during Harbin winter and Guangzhou summer (* $p < 0.05$, and ** $p < 0.01$).

According to the results of the correlation coefficient of *ESI* in Guangzhou, the $PM_{2.5}$ concentration was positively correlated with the street traffic emission, and the correlation reached its maximum value of 0.79 at 11:00 on 26 July. The contribution of street traffic to the $PM_{2.5}$ concentration in the urban blocks should not be ignored. Moreover, the $PM_{2.5}$ concentration was highly negatively correlated with *SVF* at most moments when the correlation coefficient reached its maximum value of −0.86 on 13:00 on 11 July. The maximum correlation coefficient of *AR* was 0.95, which appeared at 13:00 on 11 July. The $PM_{2.5}$ concentration and *NDVI* were mainly negatively correlated, with a maximum of −0.74 at 9:00 on 26 July. However, *HRE* and *BSF* had no significant correlation with $PM_{2.5}$ concentration on any of the test days.

Generally, the urban meteorological environment plays a major role in regulating the distributions of $PM_{2.5}$ concentration in the city blocks of Harbin. However, the influence of air temperature and humidity on $PM_{2.5}$ concentration in Guangzhou in summer is relatively limited. There is still a certain correlation between urban spatial characteristics and $PM_{2.5}$ concentration. The urban blocks with higher building area ratio, higher building height, and lower sky openness especially increase the $PM_{2.5}$ concentration in Harbin winter. For the blocks with high street aspect ratio, low sky openness, high emission intensity, and low plant coverage in Guangzhou, the deterioration of $PM_{2.5}$ is more obvious.

4.2. Curve Fitting

Results from the multi-factor analysis show the different impacts of different variables on the near-surface $PM_{2.5}$ concentration. Although the correlation relationships are expressed above, the quantitative equations illustrating the near-surface $PM_{2.5}$ concentration are needed as theoretical guidance for evaluating $PM_{2.5}$ pollution in different climates for varied urban spatial patterns and traffic emission intensities. To improve the precision of equations and the goodness of fit for better expressing the relationships between factor variables and $PM_{2.5}$ concentration, we adopted multivariate nonlinear regression models to illustrate the relationships between them. For determining the general form of the multivariate nonlinear regression model, we first discussed the suitable models for expressing each independent variable. Then, each suitable model for the factor variable was integrated into the multivariate nonlinear regression model. From the current widely used models, four typical models, namely the linear model, quadratic model, logarithmic model, and cubic model, were mainly considered to assess their applicability in describing the quantitative relationships between each factor variable and $PM_{2.5}$ concentration.

Figure 15 reflects the fitting functions between $PM_{2.5}$ concentration and factor variables during the wintertime in Harbin. A functional relationship between $PM_{2.5}$ concentration and variables other than *NDVI* can be obtained by regression. According to the fitting results of $PM_{2.5}$ concentration and air temperature, the R^2 of the quadratic curve is 0.88, which is greater than 0.56 of the linear equation. However, the equations of relative humidity, emission source intensity, and background concentration do not fit properly as their R^2 values are all below 0.3. Comparing the results of Figure 15e,f, it can be seen that the cubic curves of the $PM_{2.5}$ concentration and *SVF* can be fitted properly, and the goodness-of-fit values (R_1^2, R_2^2, R_3^2, R_4^2) are all greater than 0.5. The R-squared of the cubic curve for *AR* is close to the quadratic one. According to the results of Figure 15i,j, the R-squared values of the *HRE* cubic curves are greater than those of the quadratic curves. Comparing the results of *BSF*, the goodness of fit is better for the cubic curve, which is more appropriate for $PM_{2.5}$ prediction.

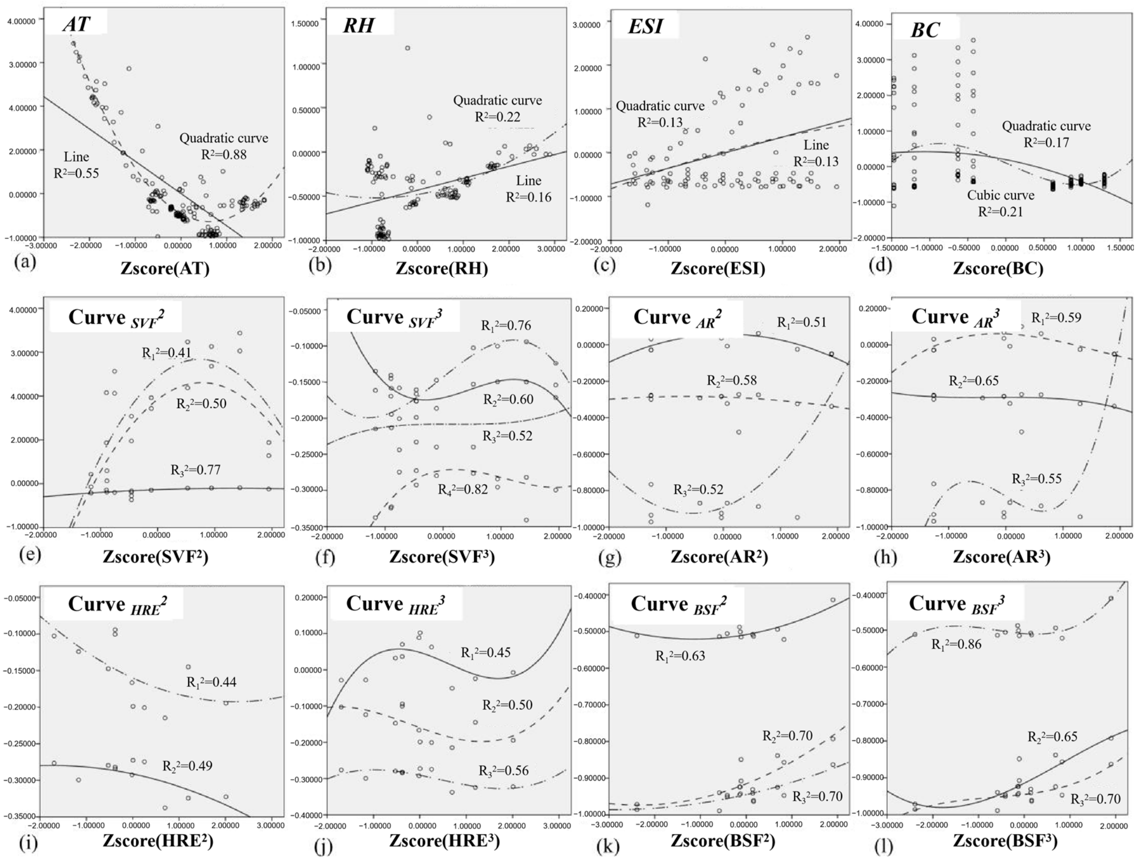

Figure 15. Fitting curves between Zscore ($PM_{2.5}$) and factors in Harbin. (**a**) Zscore ($PM_{2.5}$) and Zcore (AT); (**b**) Zscore ($PM_{2.5}$) and Zcore (RH); (**c**) Zscore ($PM_{2.5}$) and Zcore (ESI); (**d**) Zscore ($PM_{2.5}$) and Zcore (BC); (**e**) Zscore ($PM_{2.5}$) and Zcore (SVF^2); (**f**) Zscore ($PM_{2.5}$) and Zcore (SVF^3);

(**g**) Zscore ($PM_{2.5}$) and Zcore (AR^2); (**h**) Zscore ($PM_{2.5}$) and Zcore (AR^3); (**i**) Zscore ($PM_{2.5}$) and Zcore (HRE^2); (**j**) Zscore ($PM_{2.5}$) and Zcore (HRE^3); (**k**) Zscore ($PM_{2.5}$) and Zcore (BSF^2); (**l**) Zscore ($PM_{2.5}$) and Zcore (BSF^3).

As shown in Figure 16, the fit function between $PM_{2.5}$ concentration and variables other than *HRE* in Guangzhou summer can be obtained by regression. The results of air temperature and relative humidity indicate a lower degree of fit. However, the functional relationship of emission source intensity and background concentration shows better goodness of fit as R-squared values of the cubic curve of 0.65 and 0.84, respectively. Comparing the results of *SVF* from Figure 16e,f, the goodness of fit of the cubic curve is better than that of the quadratic curve. The fitting results of *AR*, *BSF*, and *NDVI* all show a better goodness of fit, and the R-squared of the cubic curve is close to the quadratic one.

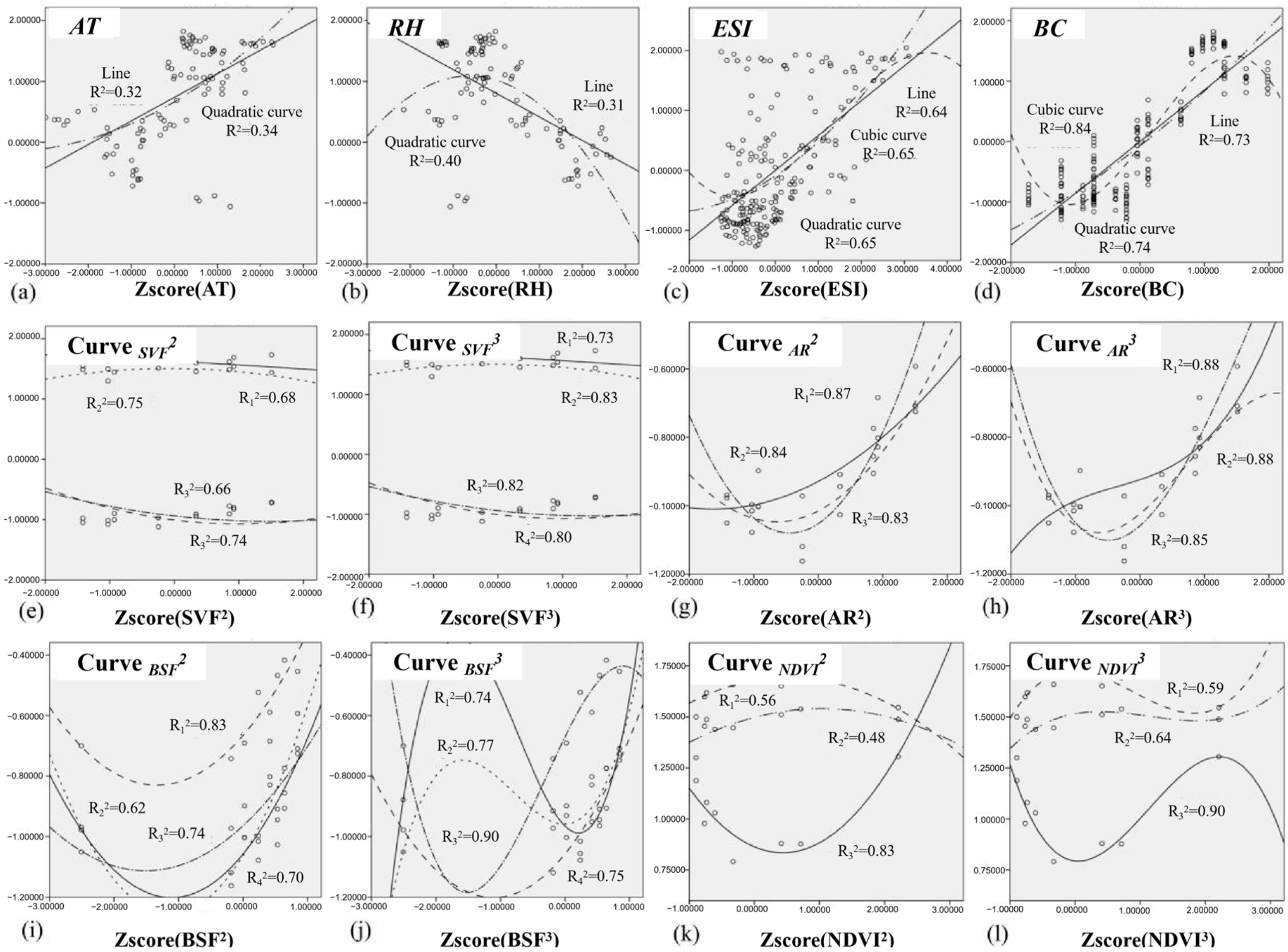

Figure 16. Fitting curves between Zscore ($PM_{2.5}$) and factors in Guangzhou. (**a**) Zscore ($PM_{2.5}$) and Zcore (AT); (**b**) Zscore ($PM_{2.5}$) and Zcore (RH); (**c**) Zscore ($PM_{2.5}$) and Zcore (ESI); (**d**) Zscore ($PM_{2.5}$) and Zcore (BC); (**e**) Zscore ($PM_{2.5}$) and Zcore (SVF^2); (**f**) Zscore ($PM_{2.5}$) and Zcore (SVF^3); (**g**) Zscore ($PM_{2.5}$) and Zcore (AR^2); (**h**) Zscore ($PM_{2.5}$) and Zcore (AR^3); (**i**) Zscore ($PM_{2.5}$) and Zcore (BSF^2); (**j**) Zscore ($PM_{2.5}$) and Zcore (BSF^3); (**k**) Zscore ($PM_{2.5}$) and Zcore ($NDVI^2$); (**l**) Zscore ($PM_{2.5}$) and Zcore ($NDVI^3$).

According to the above fitting results, the optimal fitting curve for different variables was selected to perform multivariate nonlinear fitting of $PM_{2.5}$, and Table 4 shows the comparison of goodness of fit with interaction effects. For the blocks in Harbin winter, five variables (*AT*, *SVF*, *AR*, *HRE*, *BSF*) were added to multivariate non-linear fitting. When the five fitted equations were compared, the fifth equation with five variables had higher R^2 values and lower residual error ($\delta^2 = 10.65$, $R^2 = 0.96$). For the blocks in Guangzhou summer, six variables (*ESI*, *BC*, *SVF*, *AR*, *BSF*, *NDVI*) were added to the multivariate non-linear fitting. The fifth and sixth equations with five variables had optimal R-squared values and lower residual errors (δ^2 = 14.75, R^2 = 0.93). Therefore, the $PM_{2.5}$ multivariate nonlinear fitted equations consisting of multivariate factors (air temperature, sky view factor, aspect ratio of street canyon, height of roughness elements, and the building surface fraction) in Harbin winter and traffic emission intensity, background concentration, sky view factor, aspect ratio of street canyon, and normalized difference vegetation index in Guangzhou summer were the most reasonable models in terms of goodness of fit.

Table 4. Comparisons of fitting equations evaluating near-surface $PM_{2.5}$ concentration in two climatic regions.

Near-Surface $PM_{2.5}$ Concentration	No.	Fitted Equations Covering Different Variables	Goodness of Fit	
			Residual Sum of δ^2	Adjusted R^2
$PM_{2.5}$ concentration in Harbin winter	1	$y(PM_{2.5}) = f_1$ (*AT*, *SVF*) = Curve $_{AT}{}^2$ + Curve $_{SVF}{}^3$	23.80	0.89
	2	$y(PM_{2.5}) = f_2$ (*AT*, *SVF*, *AR*) = Curve $_{AT}{}^2$ + Curve $_{SVF}{}^3$ + Curve $_{AR}{}^2$	20.97	0.88
	3	$y(PM_{2.5}) = f_3$ (*AT*, *SVF*, *AR*) = Curve $_{AT}{}^2$ + Curve $_{SVF}{}^3$ + Curve $_{AR}{}^3$	11.57	0.94
	4	$y(PM_{2.5}) = f_4$ (*AT*, *SVF*, *AR*, *HRE*) = Curve $_{AT}{}^2$ + Curve $_{SVF}{}^3$ + Curve $_{AR}{}^3$ + Curve $_{HRE}{}^3$	11.10	0.94
	5	$y(PM_{2.5}) = f_5$ (*AT*, *SVF*, *AR*, *HRE*, *BSF*) = Curve $_{AT}{}^2$ + Curve $_{SVF}{}^3$ + Curve $_{AR}{}^3$ + Curve $_{HRE}{}^3$ + Curve $_{BSF}{}^3$	10.65	0.96
$PM_{2.5}$ concentration in Guangzhou summer	1	$y(PM_{2.5}) = g_1$ (*ESI*, *BC*) = Curve $_{ESI}{}^3$ + Curve $_{BC}{}^3$	30.55	0.82
	2	$y(PM_{2.5}) = g_2$ (*ESI*, *BC*, *SVF*) = Curve $_{ESI}{}^3$ + Curve $_{BC}{}^3$ + Curve $_{SVF}{}^3$	27.69	0.85
	3	$y(PM_{2.5}) = g_3$ (*ESI*, *BC*, *SVF*, *AR*) = Curve $_{ESI}{}^3$ + Curve $_{BC}{}^3$ + Curve $_{SVF}{}^3$ + Curve $_{AR}{}^2$	22.54	0.88
	4	$y(PM_{2.5}) = g_4$ (*ESI*, *BC*, *SVF*, *AR*) = Curve $_{ESI}{}^3$ + Curve $_{BC}{}^3$ + Curve $_{SVF}{}^3$ + Curve $_{AR}{}^3$	22.54	0.88
	5	$y(PM_{2.5}) = g_5$ (*ESI*, *BC*, *SVF*, *AR*, *NDVI*) = Curve $_{ESI}{}^3$ + Curve $_{BC}{}^3$ + Curve $_{SVF}{}^3$ + Curve $_{AR}{}^3$ + Curve $_{NDVI}{}^2$	14.75	0.93
	6	$y(PM_{2.5}) = g_6$ (*ESI*, *BC*, *SVF*, *AR*, *NDVI*) = Curve $_{ESI}{}^3$ + Curve $_{BC}{}^3$ + Curve $_{SVF}{}^3$ + Curve $_{AR}{}^3$ + Curve $_{NDVI}{}^3$	14.75	0.93
	7	$y(PM_{2.5}) = g_7$ (*ESI*, *BC*, *SVF*, *AR*, *NDVI*, *BSF*) = Curve $_{ESI}{}^3$ + Curve $_{BC}{}^3$ + Curve $_{SVF}{}^3$ + Curve $_{AR}{}^3$ + Curve $_{NDVI}{}^3$ + Curve $_{BSF}{}^2$	23.65	0.87
	8	$y(PM_{2.5}) = g_8$ (*ESI*, *BC*, *SVF*, *AR*, *NDVI*, *BSF*) = Curve $_{ESI}{}^3$ + Curve $_{BC}{}^3$ + Curve $_{SVF}{}^3$ + Curve $_{AR}{}^3$ + Curve $_{NDVI}{}^3$ + Curve $_{BSF}{}^3$	23.65	0.87

4.3. Optimization Strategy

According to the research results and fitting equations, optimization strategies can be recommended to improve urban air quality in local-scale areas.

- *Optimization of urban morphology*

From an urban morphology perspective, more attention should be paid to the influence of the spatial form of urban blocks on air quality. For example, the influence of building density, the average building height, and the sky view factor on $PM_{2.5}$ should be taken into consideration in urban planning and design for Harbin. In addition, the design of urban morphology in Guangzhou should consider the influence of the street aspect ratio and the sky view factor on urban air quality.

- *Optimization of vegetation pattern*

During daily maintenance, tree planting can play an important role in regulating and reducing $PM_{2.5}$ concentration. Results show that the regulating effect of plants on the microclimate is reduced in Harbin winter as the plant coverage is low. However, in Guangzhou, with hot and humid climatic conditions, there are thick layers of plants all year round, and the plant greening coverage greatly affects the $PM_{2.5}$ concentration distribution. Therefore, more attention should be paid to the regulating effects of vegetation patterns in reducing $PM_{2.5}$ concentration in Guangzhou summer, like the vegetation layout, tree species, and configurations of plants.

- *Regional climate environment adaptability*

The climate environments of different cities present specific regional characteristics. According to the above research results, the difference in the local climate environment in the two cities has different impacts on $PM_{2.5}$ concentration. Therefore, the regional $PM_{2.5}$ regulation should adapt to the change in the local climate environment. In Harbin, where the temperature is severely cold, attention should be paid to the increase in $PM_{2.5}$ concentration caused by lower temperatures.

4.4. Limitations and Future Research

This study mainly focuses on the $PM_{2.5}$ distribution characteristics at the pedestrian level of urban blocks. Compared to current advanced spatial analysis technologies [23,24], more spatial association analysis, hot-spot/cold-spot analysis, and series of clustering characteristic analysis can be conducted in the near future. In addition, the theoretical modeling of multi-variable coupling integrated effects on $PM_{2.5}$ will be the key research points in our next research work.

5. Conclusions

This paper focuses on the spatial and temporal characteristics of near-surface $PM_{2.5}$ concentration and the corresponding driving factors. Field mobile surveys were conducted in two climatic regions. Three perspectives of factors are discussed, namely the climatic variables of background climatic conditions, five urban morphology variables, and the hourly traffic emission intensity. The relationships between near-surface $PM_{2.5}$ concentration and multiple factors are illustrated through correlation analysis.

The spatiotemporal distributions of $PM_{2.5}$ concentration were drawn through the GIS platform. Several conclusions are obtained. Results show that the distributions within the QL and PRNT urban blocks are highly diverse, both spatially and temporally. Air temperature and relative humidity are significantly correlated with $PM_{2.5}$ concentration ($p < 0.01$, correlation coefficients > 0.7) for most of the measurement times in Harbin winter. This indicates that urban meteorological environmental parameters can influence the distribution of $PM_{2.5}$ concentration. Similarly, it shows that $PM_{2.5}$ concentration may be associated with urban spatial characteristics due to the higher correlation coefficients between them. The deterioration of $PM_{2.5}$ concentration occurs in urban blocks with higher building area ratio, higher building height, and lower sky openness in Harbin and higher street aspect ratio, lower sky openness, higher emission intensity, and lower plant coverage in Guangzhou.

Multivariate nonlinear formulas were used to fit the association between these factors and $PM_{2.5}$ concentration. Higher coefficients ($R^2 > 0.8$) were obtained. This reveals that these factors can be used to predict the $PM_{2.5}$ concentration to a certain extent, which suggests that the results of this study can provide theoretical evidence for reducing air pollutants in different climatic conditions and different built-up spatial morphology with varied traffic emission intensities. In summary, this study contributes to providing field survey evidence to illustrate the driving factors of urban pollution source $PM_{2.5}$ concentration. Strategies from the perspectives of urban morphology, vegetation pattern, and background environment adaptability are suggested for environmentally friendly urban construction.

Author Contributions: Conceptualization, H.H. and J.L.; Methodology, H.H.; Validation, Z.T. and H.X. Formal analvsis L.L.: Investigation, J.W. and H.X.: Data curation, J.W.: Writing—originaldraft, Y.Z.; Writing—review & editing, L.L. and Y.Z.; Visualization, Y.Z. and Z.T.; Funding acquisition, L.L. All authors have read and agreed to the published version of the manuscript.

Funding: This work was kindly supported by the National Natural Science Foundation of China (Grant No. 52208099), Natural Science Foundation of Guangdong Province, China (Grant No. 2023A1515012161), and Guangzhou Science and Technology Plan Project (No. 202201010274).

Institutional Review Board Statement: Not applicable.

Informed Consent Statement: Not applicable.

Data Availability Statement: The data presented in this study are available in the context analysis of Sections 2 and 3 of this article.

Conflicts of Interest: The authors declare that they have no known competing financial interest or personal relationship that could have appeared to influence the work reported in this paper.

References

1. Yan, S.; Cao, H.; Chen, Y.; Wu, C.; Hong, T.; Fan, H. Spatial and temporal characteristics of air quality and air pollutants in 2013 in Beijing. *Environ. Sci. Pollut. Res.* **2016**, *23*, 13996–14007. [CrossRef] [PubMed]
2. Lin, Y.; Zou, J.; Yang, W.; Li, C.-Q. A Review of Recent Advances in Research on $PM_{2.5}$ in China. *Int. J. Environ. Res. Public Health* **2018**, *15*, 438. [CrossRef] [PubMed]
3. Luo, H.; Han, Y.; Lu, C.; Yang, J.; Wu, Y. Characteristics of Surface Solar Radiation under Different Air Pollution Conditions over Nanjing, China: Observation and Simulation. *Adv. Atmos. Sci.* **2019**, *36*, 1047–1059. [CrossRef]
4. Kant, Y.; Mitra, D.; Chauhan, P. Space-based observations on the impact of COVID-19-induced lockdown on aerosols over India. *Curr. Sci.* **2020**, *119*, 539–544. [CrossRef]
5. Zhang, S.; Routledge, M.N. The contribution of $PM_{2.5}$ to cardiovascular disease in China. *Environ. Sci. Pollut. Res.* **2020**, *27*, 37502–37513. [CrossRef]
6. Lin, H.; Long, Y.; Su, Y.; Song, K.; Li, C.; Ding, N. Air pollution and hospital admissions for critical illness in emergency department: A tertiary-center research in Changsha, China, 2016–2020. *Environ. Sci. Pollut. Res.* **2022**, *29*, 21440–21450. [CrossRef]
7. Kim, H.-B.; Shim, J.-Y.; Park, B.; Lee, Y.-J. Long-Term Exposure to Air Pollutants and Cancer Mortality: A Meta-Analysis of Cohort Studies. *Int. J. Environ. Res. Public Health* **2018**, *15*, 2608. [CrossRef]
8. Zhu, C.; Fu, Z.; Liu, L.; Shi, X.; Li, Y. Health risk assessment of PM2.5 on walking trips. *Sci. Rep.* **2021**, *11*, 19249. [CrossRef]
9. Liu, S.; Lim, Y.H.; Pedersen, M.; Jørgensen, J.T.; Amini, H.; Cole-Hunter, T.; Methta, A.J.; So, R.; Mortensen, L.H.; Westendorp, R.G.J.; et al. Long-term exposure to ambient air pollution and road traffic noise and asthma incidence in adults: The Danish Nurse cohort. *Environ. Int.* **2021**, *152*, 106464. [CrossRef]
10. Zahed, F.; Pardakhti, A.; Motlagh, M.S.; Mohammad Kari, B.; Tavakoli, A. Infiltration of outdoor PM2.5 and influencing factors. *Air Qual. Atmos. Health* **2022**, *15*, 2215–2230. [CrossRef]
11. Chen, L.; Wang, H.; Wang, Z.; Dong, Z. Estimating the mortality attributable to indoor exposure to particulate matter of outdoor origin in mainland China. *Sci. Total Environ.* **2023**, *872*, 162286. [CrossRef] [PubMed]
12. Zhang, X.; Bai, Z.; Fan, X.; Lu, Y.; Cao, Y.; Zhao, Z.; Sun, Q.; Pan, J. Urban Expansion Process, Pattern, and Land Use Response in an Urban Mining Composited Zone from 1986 to 2013. *J. Urban Plan. Dev.* **2016**, *142*, 4. [CrossRef]
13. Huang, Q.; Liu, Y. The Coupling between Urban Expansion and Population Growth: An Analysis of Urban Agglomerations in China (2005–2020). *Sustainability* **2021**, *13*, 7250. [CrossRef]
14. Krall, J.R.; Adibah, N.; Babin, L.M.; Lee, Y.C.; Motti, V.G.; McCombs, M.; McWilliams, A.; Thornburg, J.; Pollack, A.Z. Estimating exposure to traffic-related $PM_{2.5}$ for women commuters using vehicle and personal monitoring. *Environ. Res.* **2020**, *187*, 109644. [CrossRef] [PubMed]
15. Yang, Y.; Li, J.; Zhu, G.; Yuan, Q. Spatio–Temporal Relationship and Evolvement of Socioeconomic Factors and $PM_{2.5}$ in China During 1998–2016. *Int. J. Environ. Res. Public Health* **2019**, *16*, 1149. [CrossRef]
16. Zhang, H.; Wang, Z.; Zhang, W. Exploring spatiotemporal patterns of $PM_{2.5}$ in China based on ground-level observations for 190 cities. *Environ. Pollut.* **2016**, *216*, 559–567. [CrossRef] [PubMed]
17. Shith, S.; Yusof, N.F.F.M.; Ramli, N.A. Multivariate analysis on trace elements of fine particulate matter ($PM_{2.5}$) in industrial and sub-urban area. *Int. J. Integr. Eng.* **2019**, *11*, 040–052. [CrossRef]
18. Weaver, A.M.; Gurley, E.S.; Crabtree-Ide, C.; Salje, H.; Yoo, E.H.; Mu, L.; Akter, N.; Ram, P.K. Air pollution dispersion from biomass stoves to neighboring homes in Mirpur, Dhaka, Bangladesh. *BMC Public Health* **2019**, *19*, 425. [CrossRef] [PubMed]
19. Jeong, C.H.; Wang, J.M.; Hilker, N.; Debosz, J.; Sofowote, U.; Su, Y.; Noble, M.; Healy, R.; Munoz, T.; Dabek-Zlotorzynska, E.; et al. Temporal and spatial variability of traffic-related PM2.5 sources: Comparison of exhaust and non-exhaust emissions. *Atmos. Environ.* **2019**, *198*, 55–69. [CrossRef]
20. Askariyeh, M.H.; Venugopal, M.; Khreis, H.; Birt, A.; Zietsman, J. Near-road traffic-related air pollution: Resuspended PM2.5 from highways and arterials. *Int. J. Environ. Res. Public Health* **2020**, *17*, 2851. [CrossRef]
21. Li, X.; Feng, Y.J.; Liang, H.Y. The Impact of Meteorological Factors on $PM_{2.5}$ Variations in Hong Kong. *IOP Conf. Ser. Earth Environ. Sci.* **2017**, *78*, 012003. [CrossRef]
22. Zhou, Y.; Zhang, D.; Zheng, L.; Shi, R.; Chen, M. The variation characteristics of $PM_{2.5}$ in Shanghai and its correlation with meteorological factors. *Remote Sens. Model. Ecosyst. Sustain. XV* **2018**, *10767*, 181–187. [CrossRef]
23. Danek, T.; Weglinska, E.; Zareba, M. The infuence of meteorological factors and terrain on air pollution concentration and migration: A geostatistical case study from Krakow. Poland. *Sci. Rep.* **2022**, *12*, 11050. [CrossRef]
24. Zareba, M.; Dlugosz, H.; Danek, T.; Weglinska, E. Big-Data-Driven Machine Learning for Enhancing Spatiotemporal Air Pollution Pattern Analysis. *Atmosphere* **2023**, *14*, 760. [CrossRef]

25. Tan, X.; Zhou, Z.; Wang, W. Relationships between urban form and PM2. 5 concentrations from the spatial pattern and process perspective. *Build. Environ.* **2023**, *234*, 110147. [CrossRef]
26. Zhang, A.; Xia, C.; Li, W. Relationships between 3D urban form and ground-level fine particulate matter at street block level: Evidence from fifteen metropolises in China. *Build. Environ.* **2022**, *211*, 108745. [CrossRef]
27. Stewart, I.D.; Oke, T.R.; Krayenhoff, E.S. Evaluation of the "local climate zone" scheme using temperature observations and model simulations. *Int. J. Climatol.* **2014**, *34*, 1062–1080. [CrossRef]
28. Cai, M.; Ren, C.; Xu, Y.; Lau, K.K.L.; Wang, R. Investigating the relationship between local climate zone and land surface temperature using an improved WUDAPT methodology—A case study of Yangtze River Delta, China. *Urban Clim.* **2018**, *24*, 485–502. [CrossRef]
29. Jin, L.; Pan, X.; Liu, L.; Liu, L.; Liu, J.; Gao, Y. Block-based local climate zone approach to urban climate maps using the UDC model. *Build. Environ.* **2020**, *186*, 107334. [CrossRef]
30. Cheung, H.K.W.; Coles, D.; Levermore, G.J. Urban heat island analysis of Greater Manchester, UK using sky view factor analysis. *Build. Serv. Eng. Res. Technol.* **2016**, *37*, 5–17. [CrossRef]
31. Xie, X.; Huang, Z. Impact of aspect ratio and surface heating on pollutant transport in street canyons. *J. Mech. Sci. Technol.* **2007**, *21*, 1781–1790. [CrossRef]
32. Crago, R.D.; Okello, W.; Jasinski, M.F. Equations for the Drag Force and Aerodynamic Roughness Length of Urban Areas with Random Building Heights. *Bound.-Layer Meteorol.* **2012**, *145*, 423–437. [CrossRef]
33. Liu, Y.; Mu, K.; Han, B.; Zhang, M.; Bao, J.; Yang, L. Surface urban heat island effect of local climate zone. *Harbin Gongye Daxue Xuebao/J. Harbin Inst. Technol.* **2021**, *53*, 192–200. [CrossRef]
34. Bhuyan, U.; Zang, C.; Vicente-Serrano, S.M.; Menzel, A. Exploring Relationships among Tree-Ring Growth, Climate Variability, and Seasonal Leaf Activity on Varying Timescales and Spatial Resolutions. *Remote Sens.* **2017**, *9*, 526. [CrossRef]
35. Liu, L.; Lin, Y.; Wang, D.; Liu, J. An improved temporal correction method for mobile measurement of outdoor thermal climates. *Theor. Appl. Climatol.* **2017**, *129*, 201–212. [CrossRef]
36. He, H.; Zhu, Y.; Liu, L.; Du, J.; Liu, L.; Liu, J. Effects of roadside trees three-dimensional morphology characteristics on traffic-related PM2.5 distribution in hot-humid urban blocks. *Urban Clim.* **2023**, *49*, 101448. [CrossRef]
37. Rzeszutek, M.; Bogacki, M.; Bździuch, P.; Szulecka, A. Improvement assessment of the OSPM model performance by considering the secondary road dust emissions. *Transp. Res. Part D Transp. Environ.* **2019**, *68*, 137–149. [CrossRef]
38. Peng, K.; Yang, Y.; Zheng, J.; Yin, S.; Gao, Z.; Huang, X. Emission factor and inventory of paved road fugitive dust sources in the Pearl River Delta region. *Huanjing Kexue Xuebao/Acta Sci. Circumstantiae* **2013**, *33*, 2657–2663. [CrossRef]
39. Liu, L.; Lin, Y.; Liu, J.; Wang, L.; Wang, D.; Shui, T.; Chen, X.; Wu, Q. Analysis of Local-Scale Urban Heat Island Characteristics Using an Integrated Method of Mobile Measurement and GIS-Based Spatial Interpolation. *Build. Environ.* **2017**, *117*, 191–207. [CrossRef]